KfK 3633
Oktober 1984

SIMMER-II
Analyses of Expansion Phase Experiments in SNR Geometry

K. Küfner, P. Schmuck, R. Fröhlich
Institut für Neutronenphysik und Reaktortechnik
Projekt Schneller Brüter

Kernforschungszentrum Karlsruhe

KERNFORSCHUNGSZENTRUM KARLSRUHE
Institut für Neutronenphysik und Reaktortechnik
Projekt Schneller Brüter

KfK 3633

SIMMER-II ANALYSES OF EXPANSION PHASE EXPERIMENTS IN SNR GEOMETRY

K.Küfner, P.Schmuck, R.Fröhlich

Kernforschungszentrum Karlsruhe GmbH, Karlsruhe

Kernforschungszentrum Karlsruhe GmbH
ISSN 0303-4003

SIMMER-II ANALYSES OF EXPANSION PHASE EXPERIMENTS IN SNR GEOMETRY

ABSTRACT

Experiments simulating the postdisassembly expansion phase in a scaled model of a LMFBR were performed to study controlling physical phenomena and to obtain data for computer code testing and verification. After a short introduction into the safety context, the design and execution of the experiments are described. Experimental results and SIMMER-II (release 9) computer program simulations agree well for most of the integral parameters, as long as no complicated internal structures are inserted into the tank. With the perforated dip plate inserted, the quality of SIMMER-II results decreases. The reason for this behavior is discussed and some suggestions are worked out which details of the flow representation have to be improved. The influence of SIMMER-II input variations is investigated using a model problem.

SIMMER-II ANALYSEN ZU EXPANSIONS EXPERIMENTEN IN SNR-GEOMETRIE

ZUSAMMENFASSUNG

Zur Simulation der Postdisassembly Expansions Phase wurden in einem skalierten LMFBR Modell Experimente durchgeführt um die wichtigsten physikalischen Phänomene zu studieren und Daten zum Testen und Verifizieren von Computer Codes zu erhalten. Nach einer kurzen Darlegung des physikalischen Zusammenhangs werden Auslegung und Durchführung der Experimente beschrieben. Experimentelle Ergebnisse und Nachrechnungen mit dem SIMMER-II Rechenprogramm stimmen für die meisten integralen Parameter recht gut überein, solange keine komplexen inneren Strukturen in den Tank eingebracht werden. Das Einsetzen der perforierten Tauchplatten Struktur verschlechtert die SIMMER-II Ergebnisse. Der Grund dafür wird diskutiert und Verbesserungen der Hydrodynamik in SIMMER-II vorgeschlagen. Der Einfluß einiger SIMMER-II Eingabewerte auf die Ergebnisse wird durch Parametervariationen anhand eines Modellproblems untersucht.

TABLE OF CONTENTS

LIST OF TABLES

LIST OF FIGURES

1. INTRODUCTION

Hypothetical core disruptive accidents in an LMFBR may progress into a core disassembly phase if certain pessimistic assumptions are made [1]. During the progression of the energetic power excursion high amounts of thermal energy (accompanied by high pressures) are deposited in the core materials. The hot materials tend to expand using paths of lowest hydraulic resistance. During this expansion the sodium of the upper plenum will be displaced and predominantly accelerated towards the cover of the vessel. This "postdisassembly expansion phase" is investigated in this report for loop-type LMFBRs based on the SNR-300 design.

Using the results of early SIMMER-II [2] computer program simulations of the postdisassembly expansion phase an experimental program was defined and carried out in 1981 by SRI-International in close cooperation with the Nuclear Research Center Karlsruhe[3,4,9]. A similar set of experiments was conducted by SRI International for the CRBR [5] in 1978 and was analysed with SIMMER-II [6,11]. The particular features that make the recent experiments different from the CRBR experiments are the special upper core structures (e.g. much shorter in length), the inclusion of a perforated dip plate, a shield tank, and the much larger cover gas volume. Many items of importance to SNR-type reactors were thus investigated for the first time and/or in much greater detail than in the CRBR experiments. Moreover improved experimental and diagnostic techniques were used.

To support interpretation, the experiments were designed to represent the real situation in a reactor in a simple, axi-symmetric way. The approach was to simulate the expansion behavior in a 1/20-scale, transparent model (Fig.1) of the SNR-300 reactor vessel (see Table II), but the experiments are also useful for much larger (e.g. 1000 MWe) reactors if the geometrical configurations of vessel and in-vessel structures are similar (the scaling factor would then be different). The influence of various internal structures was systematically investigated by adding them successively during a series of experiments.

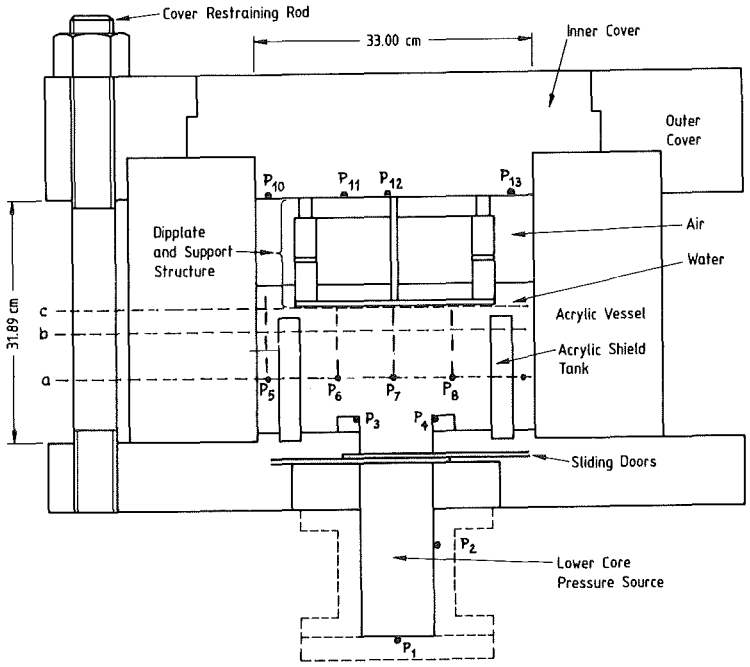

P_i : Position of pressure transducers.

The height of the inpool transducers was varied (see levels a, b, c in the sketch).

Figure 1:Schematic of the 1/20-Scale Model

The general objective was to test and verify the SIMMER-II computer code. Other more specific objectives of this experimental program were to determine:

- the growth characteristics of the expansion region ("bubble") towards the reactor cover;
- the degree of entrainment of the surrounding liquid into the expansion

region;

• the loading distribution on the primary vessel, head and internal structures for well specified driving transients (under the assumption of rigid structures);

• the characteristics of the expansion region collapse following cover gas compression and slug impact.

A summary of the experimental results may be found in [4]. In this report only the basic experiments and first experiments with an inserted dip plate are analysed.

Chapter 2 provides a short description of the design and execution of the experimental program. Chapter 3 tries to briefly characterise the SIMMER-II code. Chapter 4 gives details of the approach used to model the experiments for SIMMER-II calculations. The main results are found in chapter 5 where the calculational results are compared with the measurements. The findings of a series of parameter variations are given in chapter 6 to provide an indication of the effects of data uncertainties on SIMMER-II predictions. The last chapter lists the most important calculational problems found together with some hints how to circumvent them and/or how to improve the SIMMER-II code.

2.DESIGN, INSTRUMENTATION AND EXECUTION OF EXPERIMENTS

2.1 Design

To achieve the objectives mentioned above, simple, 1/20-scale, transparent models of the SNR-300 vessel were constructed. To help understanding of the influence of various internal structures on the expansion behavior, the configurations had increasing structural complexity. In the basic model investigated, only the shield tank was present because this structure can withstand heavy mechanical loads in the prototype. The sequence of the addition of other internal structures to the basic configuration was then selected by the mechanical stability expected under prototypical conditions. The four different configurations used are:

- basic model (including the shield tank);
- basic model with perforated dip plate (three types of dip plates with nominally 15%, 20% and 30% open flow area were used);
- basic model with dip plate (DP) and upper internal structure (UIS);
- basic model with dip plate, upper internal and upper core structure (UCS).

Fig.1 shows the model with all internal structures present . The upper internal structure of the model simulates instrumentation plate and guide tubes in the upper sodium plenum, the upper core structure simulates subassembly hexcans in the above core region of the LMFBR.

Vessel, shield tank and dip plate support structure were made of acrylic glass to make visual observations possible. Dip plate, upper internal and upper core structures were made of steel or aluminium.

Two high-pressure nitrogen sources with different volumes (732 and 11307 cm^3, resp.) were used (see Fig.2) to simulate the expansion characteristics of hot fuel and sodium. Both had a work potential of about 11 KJ for isentropic expansion to the cover gas volume (this corresponds to a work potential of about 90 MJ for the SNR-300). The high-volume 2.14 MPa source simulated a slow pressure decay comparable to prototypic cases where fuel evaporates sodium or where large masses of fuel are at a relatively high temperature (approximately 4800 K). The

TABLE I: Matrix of Experiments and Slug Impact Times

Experiment	Internal Structures DP[1]	UCS[2]	UIS[3]	Initial Pressure [MPa]	Slug Impact Time [ms]
1 & 2	No	No	No	10.0	3.37 & 3.32
3 & 4	No	No	No	2.14	5.28 & 5.24
5 & 6	20%	No	No	2.14	[4] & 6.30
7 & 8	20%	No	No	10.0	3.81 & 3.86
9	15%	No	No	2.14	6.30
10	30%	No	No	2.14	6.01
11[5]	15%	No	No	2.14	6.04
12	20%	No	Yes	2.14	6.34
13	20%	Yes	Yes	2.14	6.56
14	20%	Yes	Yes	10.0	3.94

[1]DP: Dip Plate; the numbers give the percentage of open flow area;

[2]UCS: Upper Core Structure;

[3]UIS: Upper Internal Structure;

[4]: Pressure P12 was not recorded in experiment 5;

[5]Experiment 11 was a repeat of experiment 9 with the water level above the dip plate reduced.

Time is measured from the point when the sliding doors begin to open the flow path. Slug impact times based on the pressure spike of the central pressure transducer P12 at the cover. For the first four configurations each experiment was conducted twice to assure reproducibility of the results.

low-volume 10.0 MPa source simulated a strong decay of pressure comparable to prototypic cases with a very high maximum temperature (approximately 5200 K) and a steep temperature distribution in the reactor core. Explosively accelerated sliding doors were used to release the source pressure into the vessel. By this, a fast opening time (0.5ms) and a good reproducibility were achieved. Air at atmospheric pressure simulated the cover gas. Water at room temperature was used to represent the sodium coolant.

PRESSURE SOURCE SPECIFICATION

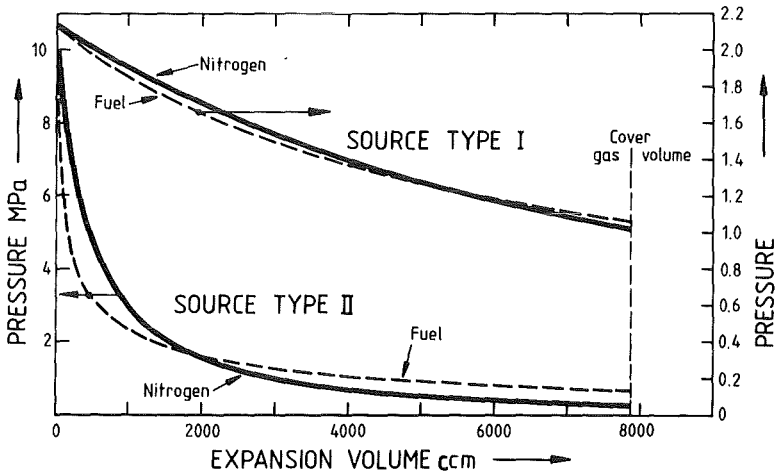

Source Isentropic Expansion Work: 11.49 kJ

Initial volumes: 732.5 and 11.307 cm³

Figure 2: Pressure Decay Characteristics of the Pressure Sources

2.2 Instrumentation

Pressure was measured in (or at) the lower core, upper core, coolant pool and vessel cover. Measurements in the coolant pool were accomplished by mounting the transducers at the tip of a stainless steel sting extending from the vessel cover. Temperature was measured in the cover gas. Strain was measured in the rods restraining the vessel cover, the dip plate support columns and in the bolts restraining the upper core structure. The vapor volume fraction was measured using

TABLE II: Scaling of Important Variables

Variable		Experiment	Prototype
Coordinates	L	1	20
Time	t	1	20
Charact. Length	1	1	20
Viscosity	μ	1	20
Displacements	δ	1	20
Velocities	v	1	1
Acceleration	a	20	1
Volumes	V	1	20^3
Pressures	p	1	1
Impulses	I	1	20
Mach No.	M	1	1
Reynolds No.	Re	1	20
Weber No.	We	1	20

conductivity probes at various locations in the coolant pool. The output of the phase probes was used to estimate the thickness of the two-phase layer at the central part of the bubble boundary.

High-speed movies (10,000 frames per second nominally) were taken of all experiments. Besides being a valuable tool for physical interpretation, these movies were digitized to quantify the bubble volume, the motion of the water surface and to get the coordinates of suspended neutral density (no slip) beads moving together with the water. This digitization was carried out only for the repeat experiments (2,4,6,8) and only up to those times where interfaces and beads were clearly visible in the movies.

The volumetric liquid entrainment in the bubble was determined after the experiment from the movie data, the impulse on the vessel cover was calculated from the cover pressure readings.

2.3 Execution

After the initial conditions in the pressure source, in the coolant pool and in the cover gas region were established and the instrumentation was checked, the experiments were initiated by igniting an oxygen-hydrogen gas mixture in the sliding door driving mechanism. The sliding doors were accelerated and after about 3.5 ms of motion they opened the core cross section rapidly (in about 0.5 ms compared to a bubble expansion time of the order of 4 to 5 ms) beginning in the center.

All experimental curves presented here are normalised in such a way that t=0 refers to the point of time when the sliding doors start to release the pressure.

At an early stage the nitrogen gas of the pressure source jetted out from the open central area, pressurized and accelerated the liquid in the upper core region. When the expanding gas reached the water pool, a gas bubble was formed. The water in the pool was displaced and accelerated towards cover gas space and reactor cover.

After the impact of the liquid on the cover a redistribution of the liquid and gas volumes took place. Depending on the geometry a number of unconnected gas and liquid volumes were created which had to combine or to redistribute before the final pressure equilibrium was established.

2.4 Discussion of Experimental Uncertainties

The mean uncertainties in measurements given in Table III were estimated by the relative deviation of trial and repeat trials wherever possible. The remaining values were taken from [3]. Impact times were resolved to the nearest 0.01 ms.

Pressure measurements were claimed [3] to be accurate within ±3% for maximum values. The errors obtained considering repeatability were considerably higher (±13%). The values given in Table III are time averaged deviations in impulse traces ($\int p dt$) calculated for the top pressure transducers (which should have the same bounds as pressures but are more convenient to evaluate). The time interval for averaging was from slug impact up to 10 ms.

TABLE III: Repeatability and Estimated Average Experimental Error

Repeatability in Experiment	1&2	3&4	5&6	7&8	Error
Measurements %					
Impact Times	1	1	-	1	1
Impact Pressures	3	5	-	12	7
Peak Pressures	3	3	-	5	4
Pressures	14	7	-	17	13
Derived Quantities %					
Impulse to the Head	15	2	-	12	10
Displaced Volumes	-	-	-	-	10
Kinetic Energy	-	-	-	-	40
Bubble Expansion Work	4	6	-	4	5

Repeatability was defined as the relative deviation of variables in trial and repeat. For experiments 5&6 no such comparison was possible because the top pressure transducers were not mounted in 5. The table shows absolute values.

Displaced volumes were calculated by digitizing the movement of suspended neutral density beads (I) above the upper core outlet and by digitizing the movement of the upper water surface (II) and were accurate to ±10% each [3]. But method I is more reliable for the early times (say 1 to 1.5 ms), method II is more accurate later on. The results (displaced water volumes, kinetic energies) presented here all used the values of method I. Velocities were calculated using differences of displaced volumes, so they had an error of at least ±20%. Since they entered by square into kinetic energy, this quantity had an error in excess of ±40%. Note that this bound did not include approximation errors in the kinetic energy estimation procedure. For reasons of accuracy the evaluation of kinetic energies based on

displaced volumes after method I was stopped whenever the displacements estimated by I and II started to deviate by more than ±10 %[+)].

The values in the last column of Table III will be referenced as the error associated with the measurements of the relevant variables in comparing with calculations.

+) To calculate kinetic energies over a larger period of time one would have had to switch from method I to method II at some point of time. However, that was not done in the experimental evaluations.

3. SHORT CHARACTERISATION OF THE SIMMER-II CODE

The SIMMER-II code [2] is a twodimensional multifield, multicomponent, Eulerian fluid dynamics program including neutronics feedback using either point kinetics, neutron diffusion or neutron transport theory. The thermal hydraulic equations are supplemented by general exchange functions for mass, momentum and energy transfer. The principle objective is to predict long term material motions in disrupted LMFBR systems. A variable Eulerian mesh is used to discretise the equations.

The fluid-dynamics equations in SIMMER-II are treated with the IMF (Implicit Multifluid Field) method. Two different velocity fields are calculated (one containing gaseous, the other fluid components). Each field is composed of several components, such as fuel, coolant, fission gas, steel. In addition a structure field is introduced to model solid fuel, cladding and subassembly can walls. This structure field is fixed in space and acts like in infinite momentum sink. It is frequently used in our SIMMER-II calculations to represent the complicated boundaries of the experimental geometry.

The basic flow regime is dispersed droplet flow, but also single-phase gas or liquid flow can be represented. Surface tension effects are taken into account only for the droplets. Some inconveniencies, inaccuracies and inefficiencies are connected with the modelling of structures because SIMMER-II supposes interpenetrating flow in each computational mesh cell. For mesh cells containing physically only structural materials one has to specify therefore a small liquid (or gas) content. Pressure and fluid flow is calculated for such mesh cells also. The flow can be stopped using very high friction factors.

All calculations reported here used the standard SIMMER-II release 9 (URANUS option). Typically somewhat more than one hour CPU time was spent per calculation on a SIEMENS 7890 computer (equivalent to 3 hours on IBM/370 M3033) for a 10 ms range of problem time and about 780 mesh cells.

4.MODELLING OF THE EXPERIMENTAL SETUP IN SIMMER-II

4.1 Generalities

SIMMER-II (release 9) calculations had been performed for the baseline experiments (no.1 to 4) and the experiments with the 20% open perforated dip plates (no.5 to 8). A 2d cylindrical geometry mesh with azimuthal symmetry was used to model the experimental apparatus (see Fig.3.a.). The spacing of the calculational mesh used generally had been of the order of 1 cm, axially somewhat larger in the pressure source regions (~20 meshes radially and ~40 axially; see Fig.3.b.). Changes in the mesh spacings were neccessary at some places to represent the dimensions of the model correctly. Some care was used to change the spacing of adjacent cells by at most a factor of 2. The initial temperature was 293 K uniformly over the model. Heat transfer processes were suppressed by input specification. A mesh cell was treated as single phase cell if there was less than 2% gas in it (input variable ALPHA0). The particle interference effect exponent (variable PIEE) was set to 3 to model a rather tight momentum coupling of liquid and vapor field. Most of the other input variables used the SIMMER-II defined default values. See App. A for a typical input set. See chapter 6 for the effects of parameter variations. [4,7] contain results of earlier calculations; the results presented here are improved in some respects.

4.2 Water Pool

The water in the experiment was represented using the liquid field component sodium in SIMMER-II input (see Table IV). Appropriate input constants had to be provided for the SIMMER-II sodium equation of state. The mesh cell type 7 ("no structure in cell") was used. A small fraction of water vapor and nitrogen (2%) was added in those cells because SIMMER-II requested a positive void fraction for these pool cells.

4.3 Pressure Source

Nitrogen in the pressure sources of the experiment was modelled using the SIMMER-II fission gas component of the vapor field (i.e. as

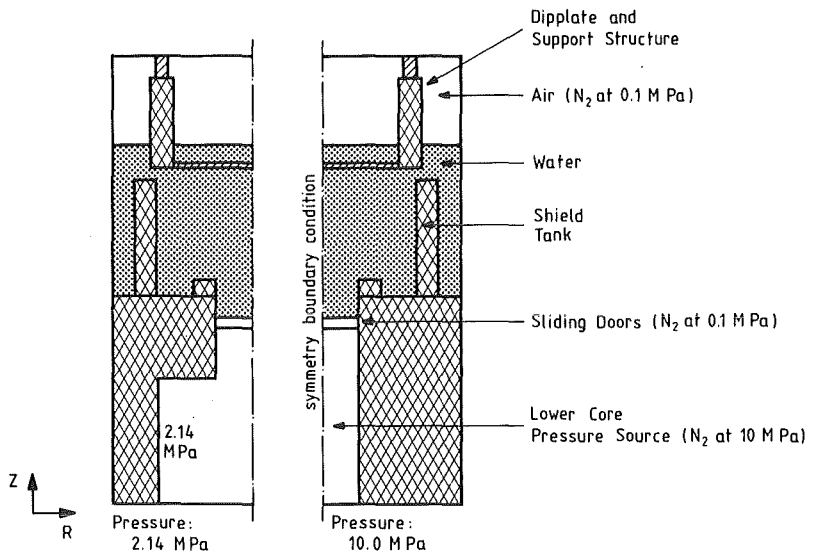

Figure 3.a: SIMMER-II Model of the Experimental Apparatus

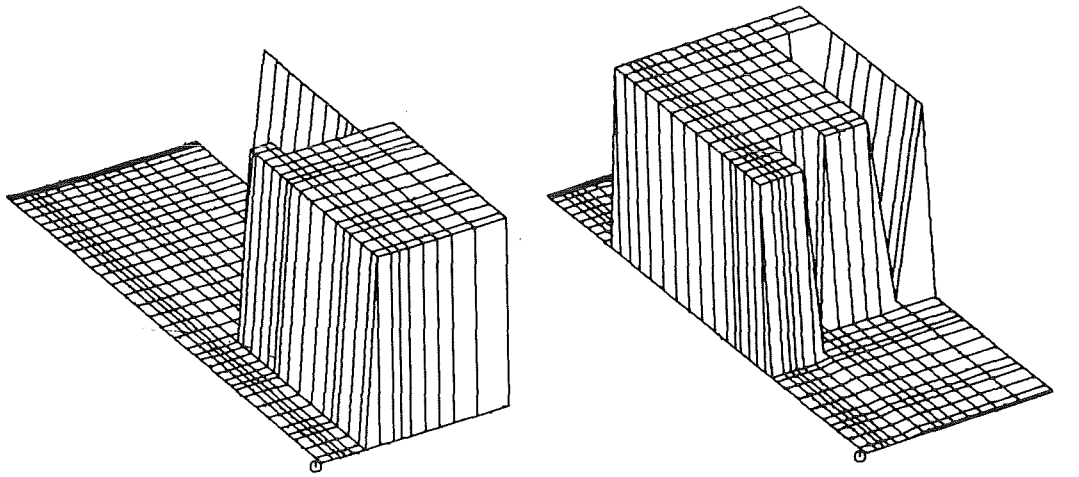

Volume Fraction of Solid Field

Volume Fraction of Liquid Field

Figure 3.b: Typical Calculational Mesh (used for Experiment No.1)

noncondensible gas) with appropriate input values for the equations of state. The experimental initial pressure of 2.14 MPa and 10.0 MPa resp., was maintained. Again, these regions were modelled with no structure in the cell and with a small liquid fraction.

4.4 Cover Gas Region

Air in the cover gas of the experiment was modelled using the SIMMER-II fission gas component of the vapor field (i.e. as non-condensible gases) with appropriate input values for the equations of state. In essence, the same description as for the pressure source regions was used with hydraulic diameters and initial pressures changed. Some fine meshes below the head were added to improve the accuracy of slug impact.

4.5 Sliding Doors

The sliding doors (separating the pressure source from the water pool) were modelled as a nitrogen zone of atmospheric pressure, by which they were assumed to open instantaneously[+)]. The real doors needed approximately 0.5 ms to be fully open. The following procedure was used to compare SIMMER-II simulations with experimental data: a synchronisation of experiments with the SIMMER-II calculations was enforced at the time when the water initially in the upper core (between the sliding doors and the pool) had been expelled into the pool. This procedure allowed circumventing a detailed simulation of the sliding doors (and also compensated partly for a numerical error of SIMMER-II calculations leading to a somewhat large expulsion time [8]). The synchronisation enabled a comparison for: progression of the expansion zone into the pool region, impact on the cover and evolution of the collapse phase. For the very early expansion phase (say the first 0.2 ms) comparisons are not so meaningful. Table V shows that the adjustments normally were fairly small. Using a more refined door opening model in the calculations would have shifted t_{CA} to later times and one would have obtained bigger synchronisation adjustments.

+) See [6,11] for alternate, much more detailed simulation of the opening sequence.

TABLE IV: Input to SIMMER II for the Calculations

Experimental Material	SIMMER II Component
H_2O(coolant)	Sodium[1]
N_2 (pressure source)	Fission gas[1]
Air (cover gas)	Fission gas[1]
Steel	Steel (can/clad)[2]
Acrylic glass	Steel (can/clad)
Sliding doors	Fission gas[1]

[1]: Appropriate input of constants for the equations of state were provided; the constants are givven in App.A, "MATERIAL PROPERTIES AND EQUATION OF STATE DATA", page 49.

[2]: The perforated dip plates were modelled as can/clad structures with appropriate open flow area; see Chapter 4.6 and App. A.

4.6 Dip Plate

The dip plate has been modelled as a porous structure using can and clad material with a bigger open flow area than in the experiments. The percentage increase for the open flow area was based on experiences gained with one dimensional model calculations [9]. The porosity of the dip plate had to be increased to give correct mass flow rates in benchmark problems (25% increase for the dip plate under investigation with a nominal open flow area of 20%; more generally: the range of increase extended from 10 to 50% depending on the original nominal open flow area [9]). To simulate the irreversible pressure losses at the dip plate the SIMMER-II orifice model was used with an appropriately adapted orifice coefficient.

TABLE V: Synchronisation Time Adjustments for the Calculation

	Exp.2	Exp.4	Exp.6	Exp.8
Emptying time[1] [ms]				
Experiment (t_{Ex})	0.933	2.012	1.988	1.156
SIMMER-II prediction (t_{CA})	1.000	2.069	2.037	1.024
Adjustment to synchronise experiment and calculation in [ms] ($\Delta t=t_{Ex}-t_{CA}$)	-.067	-.057	-.049	+.132

[1]: of upper core barrel; times calculated for the experiment refer to the beginning of the door opening and used the displaced water volume estimated by neutral bead movement; in the SIMMER-II calculations, the doors were assumed to be totally open at t=0.0; the volume of gas in the expanding bubble was used to determine the displaced volumes of water.

4.7 Rigid Structures

Internal rigid structures (as shield tank and dip plate support structure) were represented by a mixture of can and clad steel which was effectively impermeable for gas and liquid field (drag set to infinity). As the movies showed, some bending occured, very late in the expansion, for the shield tank cylinder and its support structure. The effect of this bending had not been investigated in our model because the total internal volume of the vessel did not expand and the outer acrylic vessel walls were not deformed.

5.CALCULATIONAL RESULTS

5.1 Generalities

Experiments 1 to 8 were a series of experiments where each experiment was followed by an repeat trial. Only these repeats were considered for the comparison because they have been evaluated in greatest detail. Comparison of data and calculation should be seen in the frame of experimental uncertainties (see Table III). We will state that SIMMER-II reproduced the experiments very well if the deviation is within those bounds stated in Table III. A reasonable agreement will be achieved if the deviation is at most twice the error indicated there for the relevant variable. A summary of the evaluation procedure used may be found in Appendix B.

5.2 Impact Times

Table VI compares the impact times of experiments and calculations. Impact times are based on the pressure spike recorded from the top central pressure transducer position P12[+)]. The repeatability of impact times in the experiment was good (deviation approximately ±1%, see Table I, III). The calculated impact times generally showed some delay and were off at most 6% from experimental values. Only for experiment 2, impact was earlier in the calculation.

5.3 Pressures

Figs.4 compare the of pressure traces at some selected positions.

The pressure decay characteristic was well reproduced (Figs.4 a,b) for both sources. Note, that for the high pressure source experiments some gas was leaking out before the sliding doors really opened the flow

---

[+)] One could have estimated impact times ([3]) by the first sharp rise of the pressure curve for P12. This would improve a little bit the agreement between experiment and calculation but as Figs.4 g-j show, it is difficult to exactly define this "sharp rise" for the calculational results.

TABLE VI: Impact Times, Pressures, Impulses and Peak Pressures

	Exp.2	Exp.4	Exp.6	Exp.8
Impact Times[1] [ms]				
Experiment	3.32	5.24	6.30	3.86
SIMMER-II Prediction	3.13	5.36	6.58	3.87
Impact Pressures [MPa]				
Experiment	34	20	10	20
SIMMER-II Prediction	15	8	5	4
Impact Impulses[2] [kN*ms]				
Experiment	157	207	108	144
SIMMER-II Prediction	135	110	67	97
Impact Impulse Trace[3] [MPa*ms]				
Experiment	3.61	3.29	2.40	2.83
SIMMER-II Prediction	3.62	3.03	2.24	3.37
Peak Pressures[4] [MPa]				
Experiment	34	20	13	35
SIMMER-II Prediction	23	22	12	8

[1]: Time in experiments is measured from the point when the sliding doors begin to open the flow path. Slug impact times and pressures are determined according to the pressure spike of the central pressure transducer at the cover.

[2]: This is the contribution of the impact pressure spike to the total impulse on the vessel head; calculated as the difference of the impulses at the beginning of the sharp pressure rise and the corresponding value 1 ms later in time.

[3]: $\int p\,dt$, calculated in a similar way as the Impact Impulse.

[4]: $P_{peak}(t) = \max \{ P(r,t'), r \text{ on cover head}, t' \leq t \}$; see also text below.

path reducing the initial pressure to approximately 9 MPa; in the 2.14 MPa experiments no such effect was observed, presumably because the source volume was 10 times bigger and the initial pressure much lower.

Figs. 4 c-f compare the pressure readings for some positions in the pool (the locations of the transducers are indicated in Fig.1). The trend of the experimental curves was generally reasonably predicted. Strong oscillations in the early phase of the calculation were correlated to the accelerated liquid before the bubble interface passed the transducer position. The pressure peak at the time the bubble interface arrived at the transducer was overpredicted in the calculations (see Fig.4 c-f).

Figs. 4 g-j show the impact pressure curves for the top central transducer (P12).

In all calculations, impact occured with a less steep gradient than in the experiments. The amplitudes of pressure spikes at slug impact was not well reproduced (see Table VI)[+): in the calculation the amplitude was low by a factor 2 to 3; in experiment 8 there was even a factor of 5. In this case, however, the reproducibility of the experimental values (normally achieved within ±5%) was poor (see Table III). Note that the second peak is reproduced considerably better in that case (see Fig.4j). These high discrepancies might be attributed to numerical diffusion and smearing effects [12] inherent to the SIMMER-II fluid-dynamics algorithm. By this diffusion mechanism the mesh cell adjacent to the cover wall was filled earlier but with less liquid than in experiments, so that the water surface was smeared out. A water hammer effect seen in the experiment could not be well reproduced with SIMMER-II.

Peak pressures on the head, calculated as

$$P_{peak}(t) = \max \{ P(r,t'); \; r \text{ on cover head}, \; t' \leq t \},$$

agreed much better (see Fig.6 and Table VI) except for experiment 8. However, a full comparison of experimental and calculated values is not possible for this variable because the SIMMER-II maxima were estimated

---

+): in contrast to the findings of [11]. We suppose that the (10 times) larger cover gas volume in our experiments and the larger time scales were the reason for that.

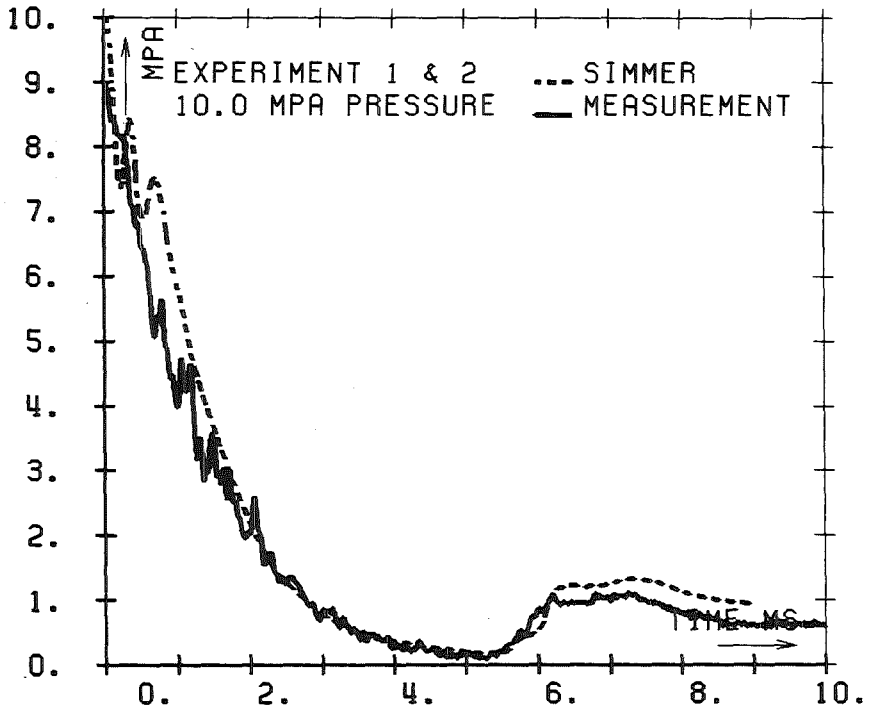

Figure 4.a: Pressure at Position P2

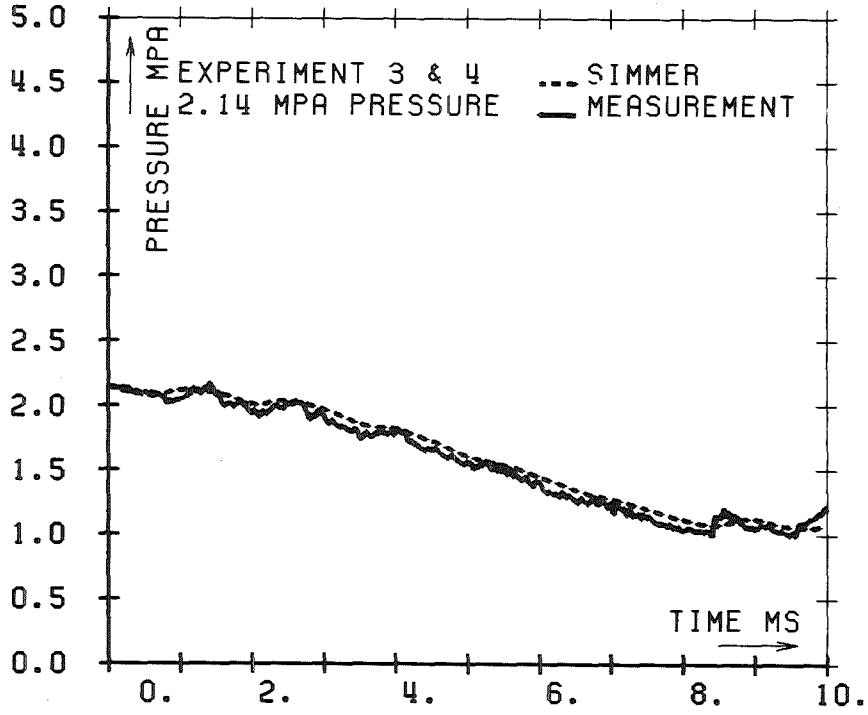

Figure 4.b: Pressure at Position P2

Figure 4: Pressure Traces at Selected Positions

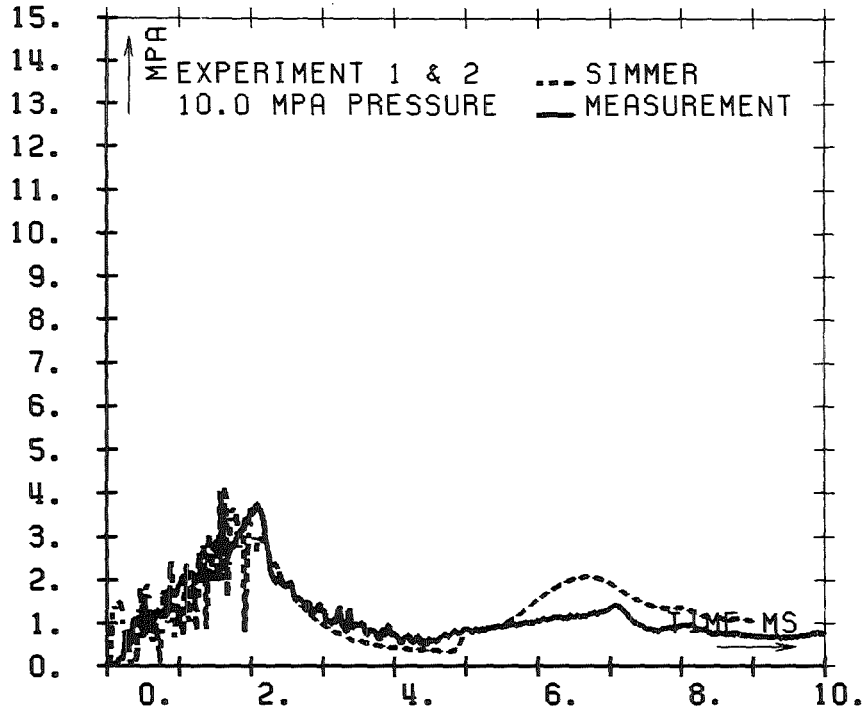

Figure 4.c: Pressure at Position P7b

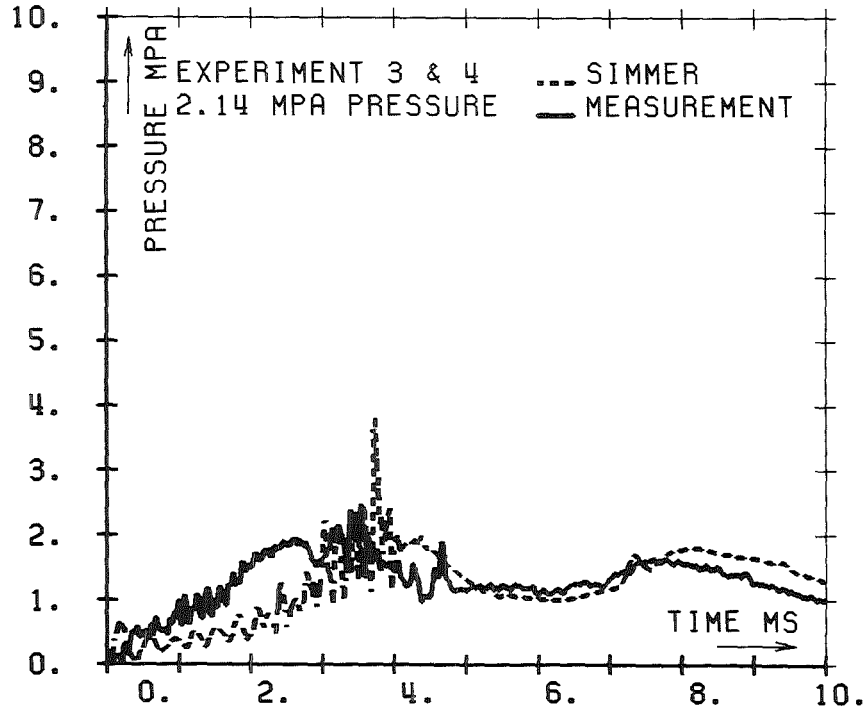

Figure 4.d: Pressure at Position P7b

Figure 4 (cont.): Pressure Traces at Selected Positions

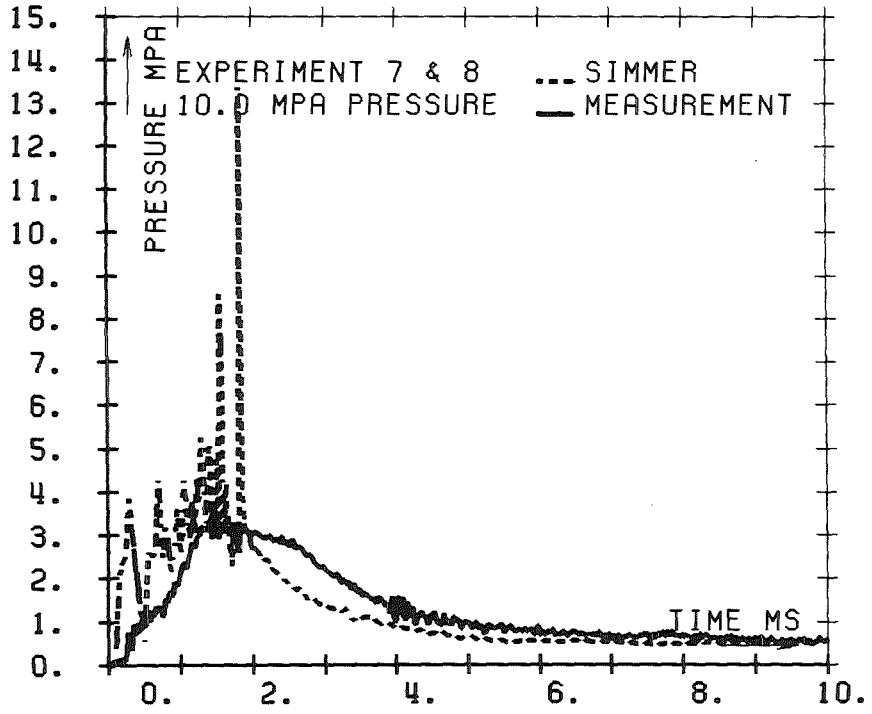

Figure 4.e: Pressure at Position P7a

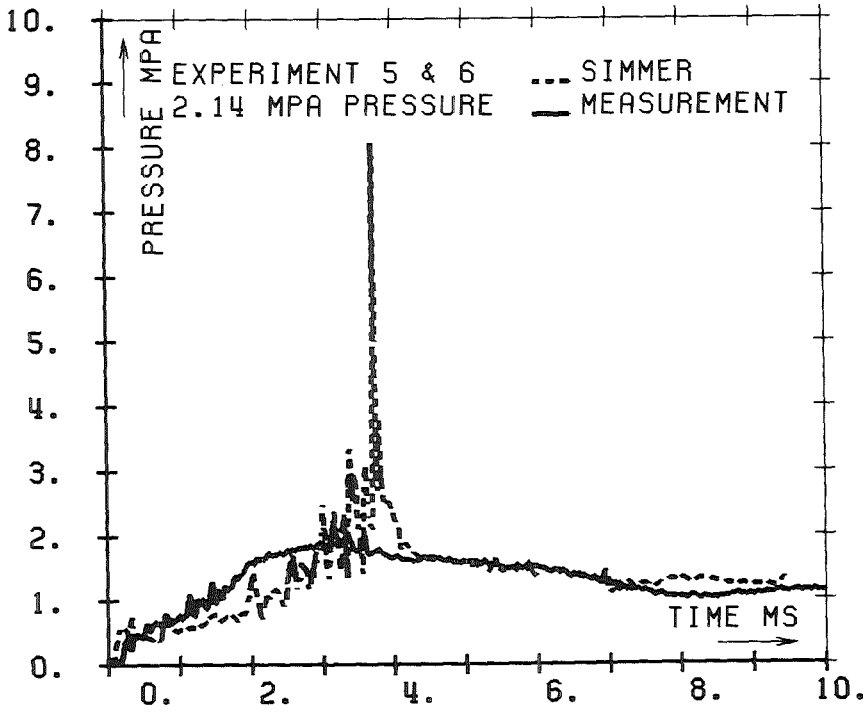

Figure 4.f: Pressure at Position P7b

Figure 4 (cont.): Pressure Traces at Selected Positions

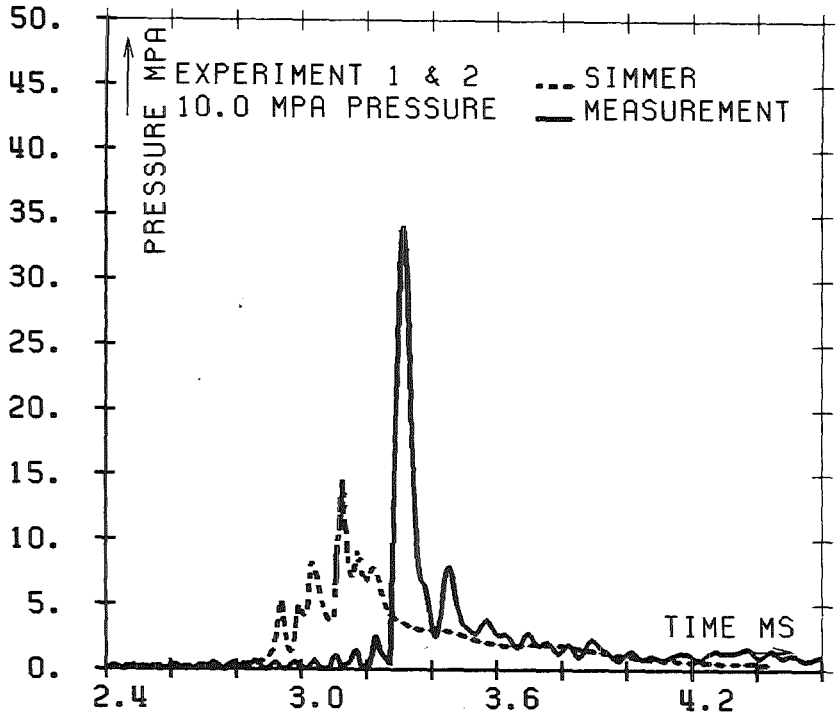

Figure 4.g: Pressure at Position P12

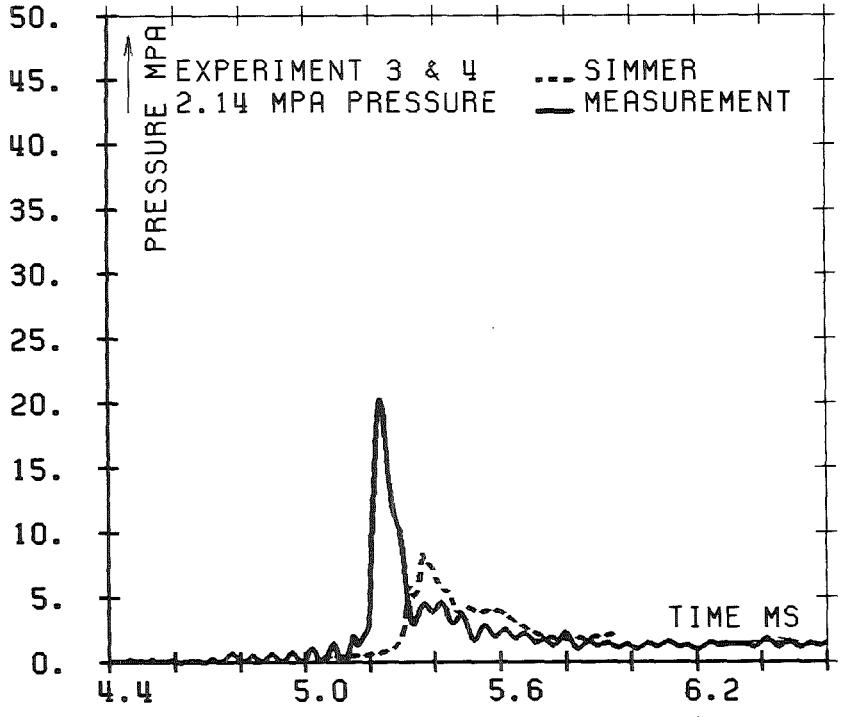

Figure 4.h: Pressure at Position P12

Figure 4 (cont.): Pressure Traces at Selected Positions

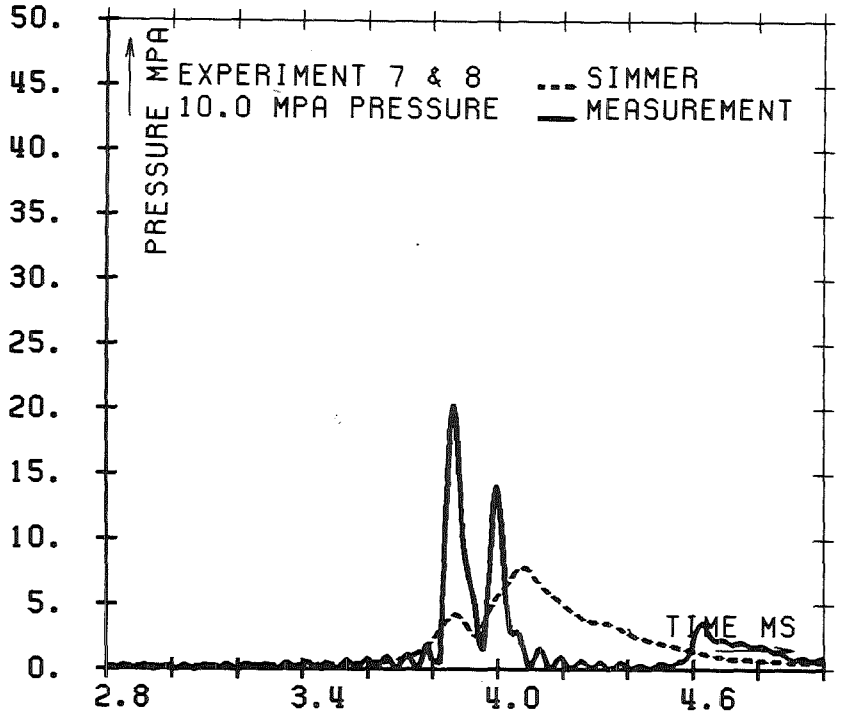

Figure 4.i: Pressure at Position P12

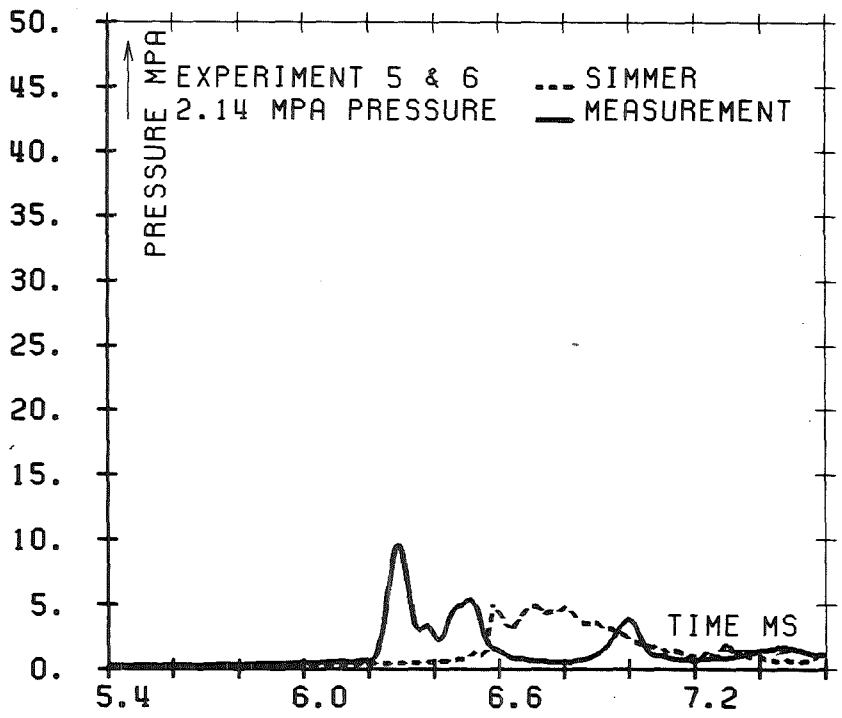

Figure 4.j: Pressure at Position P12

Figure 4 (cont.): Pressure Traces at Selected Positions

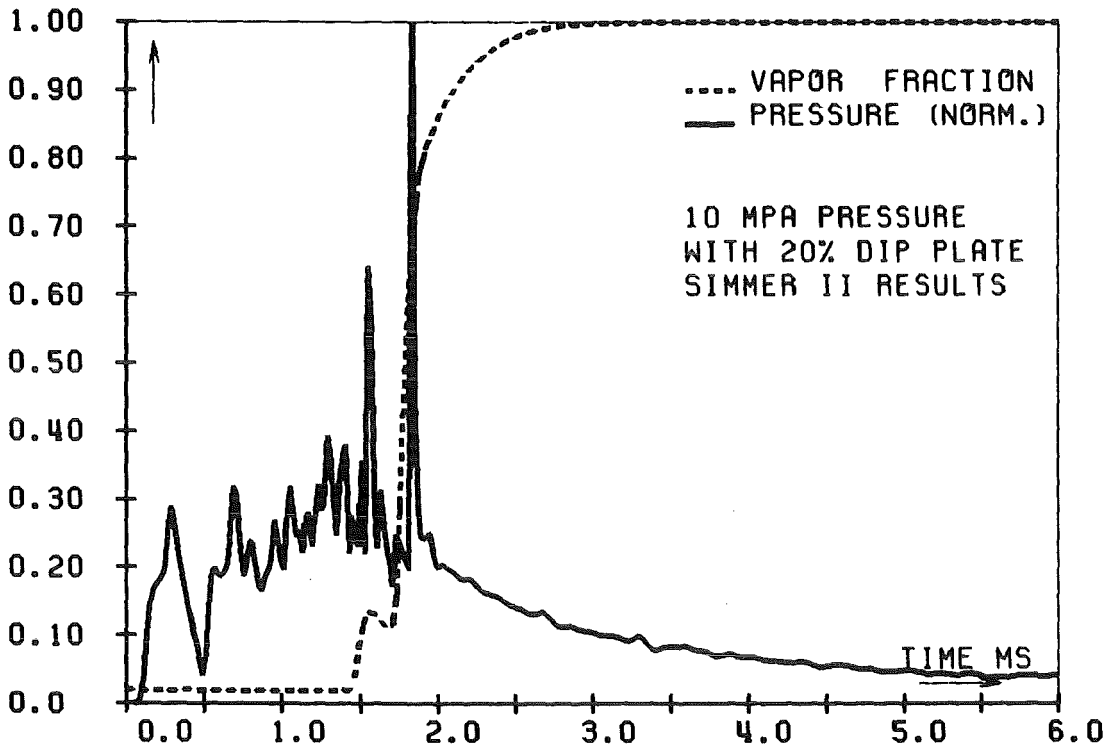

This figure shows the SIMMER-II calculated pressure from Fig.4.e normalised to maximum value 1.0. The second variable represents the calculated vapor volume fraction at the same location.

Figure 5: Correlation Between Pressure and Vapor Volume Fraction

using approximately 20 radial positions whereas the experimental observations used only three. In the low pressure experiments the peak pressure developments showed some time delay.

5.4 Impulse to the Head

The impulse traces ($\int pdt$) for the top pressure transducers deviated at most by ±20% in the late phase. For the low pressure experiments the deviations were even considerably smaller. In the early phase up to slug impact the experimental values were overestimated by a factor 2-3 but during that time the measured pressure values below the roof were very inaccurate [8]. The qualitative behavior of impulse traces was reproduced very accurately.

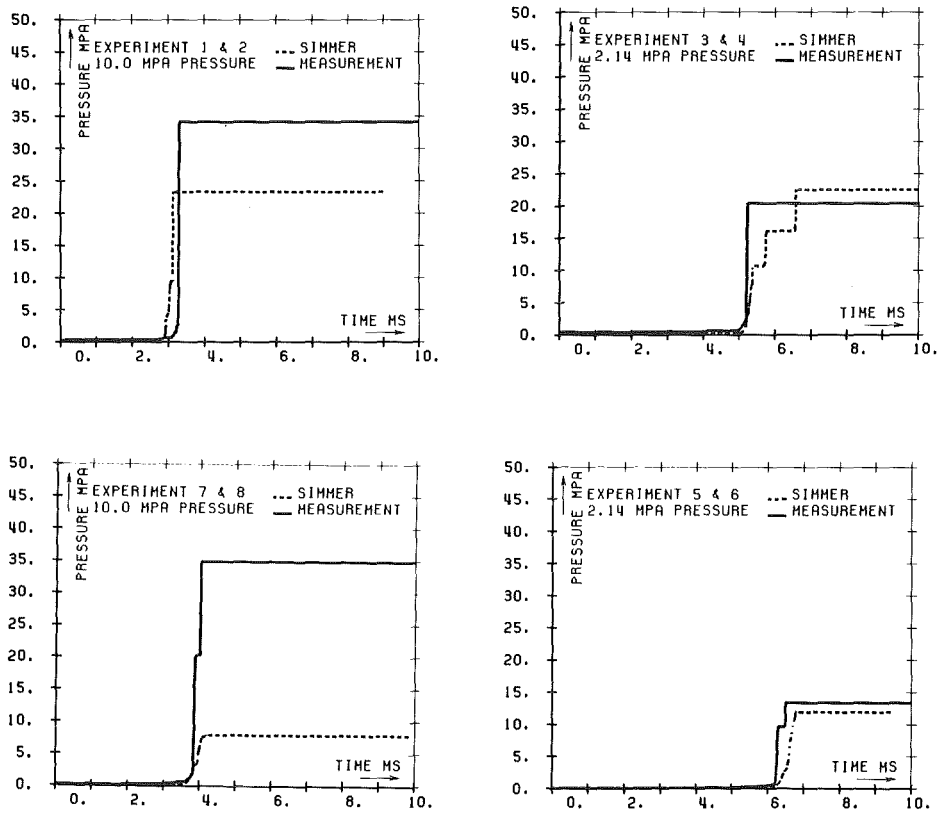

Figure 6: Peak Pressures on the Head (see text below!)

The values for the impact impulse trace are the contribution of the impact pressure spike to the impulse trace curve. They were calculated as the difference of the impulse traces at the beginning of the sharp rise of the pressure curves given in Figs.4g-j, and the value 1 ms after that time. The much too low impact pressure amplitude in the calculation was compensated by the much broader peak so that we had a good agreement between experiment and calculation (see Table VI, row 4).

The total impulse delivered to the cover head was calculated by

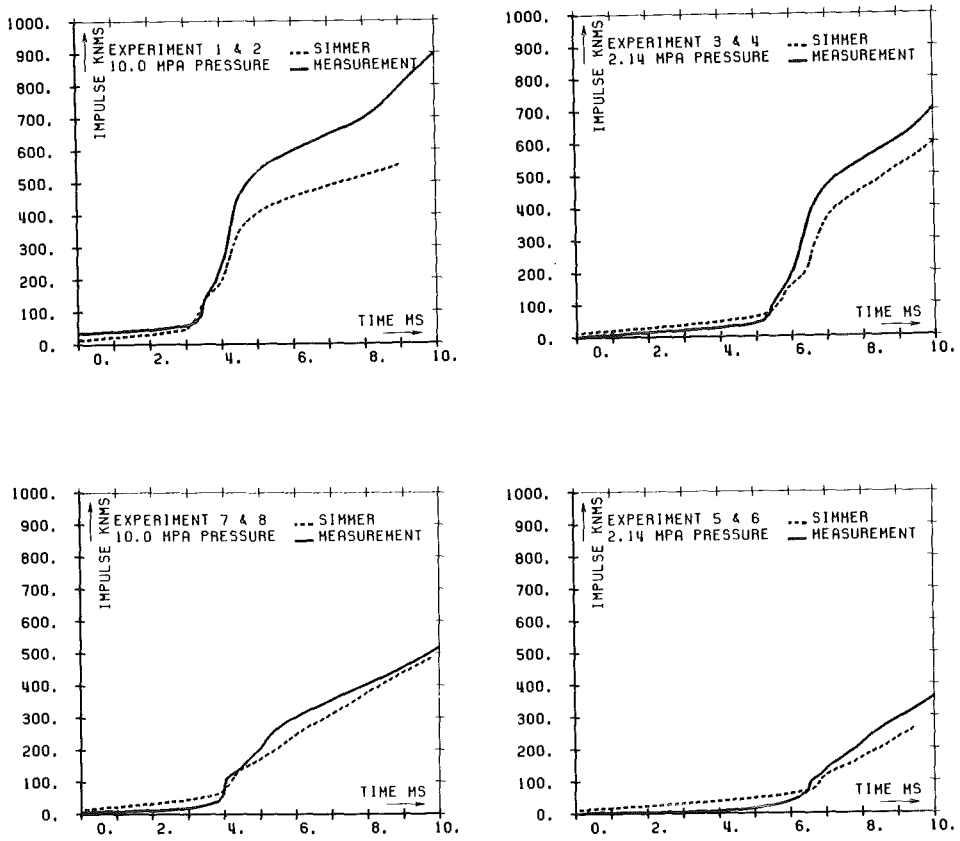

Figure 7: Impulse to the Head

$$I_{tot}(t) = \int \Sigma_i A_i P_i(t')dt',$$

where the range of the integral extended from time 0 to t and A_i was a fixed area partition of the cover.

In SIMMER-II evaluations this partition coincided with the calculational mesh structure. In the experiment only three pressure readings had been recorded at the cover, and therefore a much higher discretisation error was involved[+)]. Studies [10] had shown that all meaningful partitions in

essence gave comparable impulse behavior but one should keep in mind that the approximations for evaluating the impulse out of the pressures measurements were rather crude. Fig. 7 shows that for the range up to 10 ms the total impulses to the head agreed to within 10 to 20% in experiments 3 to 8. A small pressure peak of the rightmost top transducer in experiment 2 caused a further rise in the impulse curve after about 8 ms, because the area associated with this transducer was so big. Since this peak could not be reproduced by SIMMER-II, the impulse curve showed a growing deviation in that case for the late phase (but the deviation is still in the range of 20 - 25%).

The impact impulses given in Table VI were calculated in the same manner as the impact impulse traces (see discription above). The numbers showed that also for this variable the agreement is not so good (deviations between 16% and 88%). Numerical diffusion caused the total impulse to be rather high even before impact; in the experiments., pre-impact impulses were negligible, however. Moreover, the calculated post-impact impulses had a smaller gradient than the experimental ones. In calculating the impact impulses as differences of post- and pre-impact impulses, this numerical deficency caused a relatively high deviation of experimental and calculated results.

5.5 Displaced Volumes

Fig.8 displays the time development of the displaced volumes in the experiments derived from the digitized movement of the neutral density beads and the volume calculated from SIMMER-II results using the gas volume of the expanding bubble. The digitized volumes were estimated [3] to be accurate within ±10%. For all experiments except 8, the curves agreed very well.

+) Unfortunately it was not possible to calculate impulses from the strain gages mounted in the roof support structures because these measurements were distorted by stress waves resulting from the experiment initiation and opening of the sliding doors.

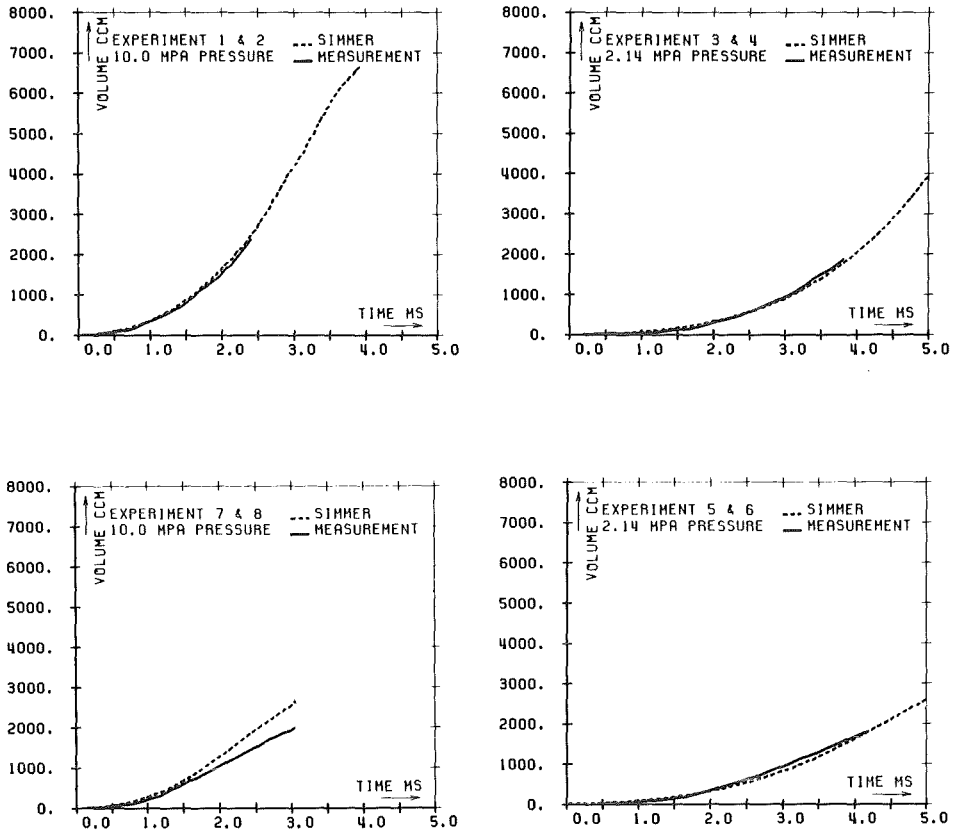

Figure 8: Comparison of Displaced Water Volumes

5.6 Energies

The uncertainties in the experimental values of kinetic energies were difficult to estimate. These values were derived under the assumption that the liquid could be partitioned into several rectangular slugs moving with velocities compatible with mass conservation. Visual records show, however, that this was not a good model to represent local flow, especially at the later expansion times. An elementary

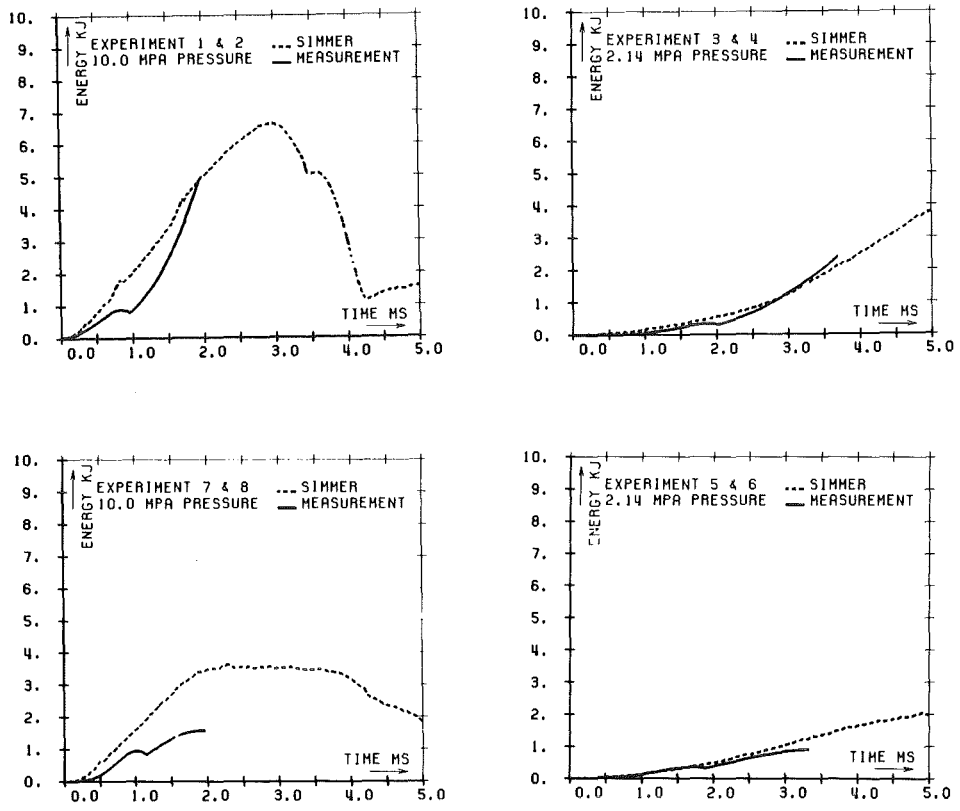

Figure 9: Kinetic Energies of the Coolant

consideration of the evaluation procedure showed that the uncertainty in displaced volumes caused an error of about ±40% in kinetic energies (see Chapter 2.4, Table III).

In Fig.9 the development of the kinetic energy with time is plotted. SIMMER-II overpredicted the kinetic energies in general. This had to be expected because SIMMER-II does not account for important dissipative fluid-dynamics effects (e.g. vortices). For the dip plate experiments, larger deviations developped at later times, the increase

TABLE VII: Comparison of SIMMER II Results for Energy Conversion with Experimental Values

	Units	Exp.2	Exp.4	Exp.6	Exp.8
Expansion time[1]	[ms]	1.691	3.277	3.243	2.137
Expansion (displaced) Volume	[ccm]				
Experiment		1113	1213	1132	1171
SIMMER-II prediction		1119	1154	1012	1470
Kinetic Energy of Liquid	[KJ]				
Experiment		3.38	1.67	0.89	-
SIMMER-II prediction		4.21	1.62	1.22	3.49
Bubble Expansion Work	[KJ]				
Experiment		5.88	2.57	2.42	6.03
SIMMER-II prediction		5.89	2.46	2.19	6.70
Cover Gas Compression Work	[KJ]				
Experiment		0.12	0.14	0.13	0.13
SIMMER-II prediction		0.14	0.13	0.11	0.18
Energy Conversion	[%]				
Experiment		58	69	39	-
SIMMER-II prediction		72	69	59	54

[1]The expansion time for the comparison was chosen in such a way that the experimental displaced volumes had a comparable size.

Bubble expansion work up to cover gas volume: approximately 11 KJ for all experiments.

of the experimental values being much smaller than the increase in calculated values. The complicated mixing behavior of the liquid above the dip plate and in the outer annular space (between the dip plate support structure and the vessel wall) as well as the high uncertainty in experimental data is believed to be sufficient to explain these deviations.

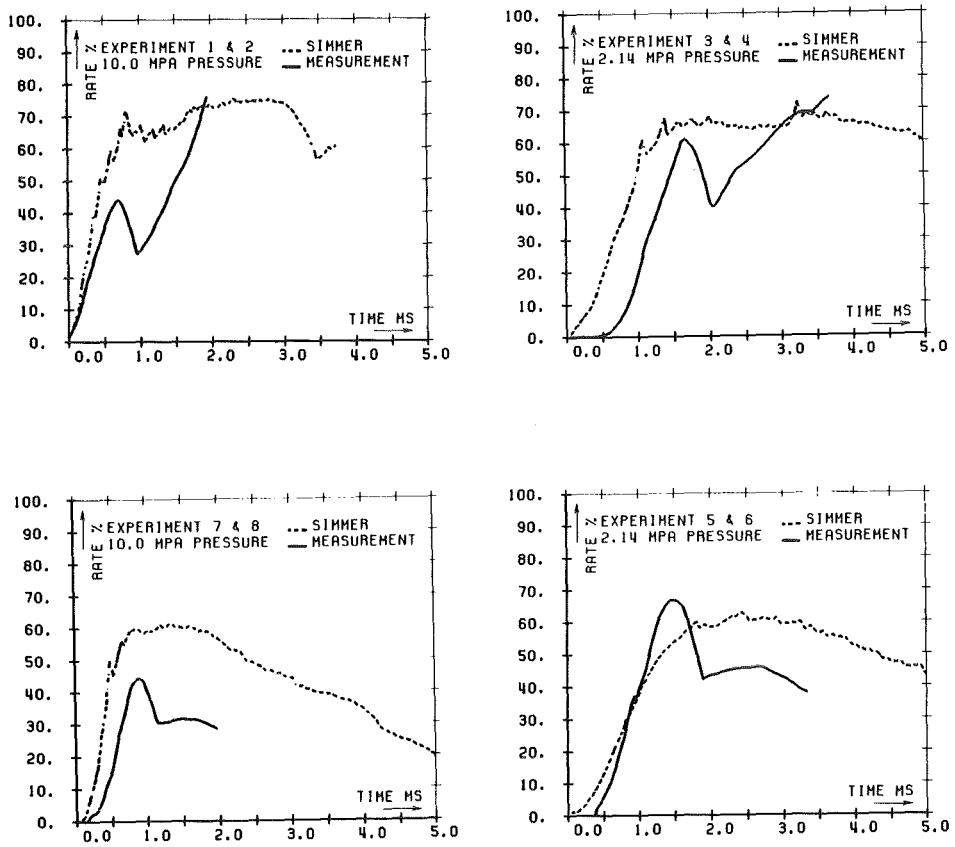

Figure 10: Conversion of Bubble Expansion Work to Kinetic Energy

In Table VII the efficiency of energy conversion[+)] is compared for SIMMER-II results and evaluated experimental data. The expansion work was dissipated in SIMMER-II simulations less effectively than in the experiments (see Fig.10).

[+)] Conversion is defined as the ratio of kinetic energy of the water over the difference between bubble expansion work ($\int pdV$) and cover compression work.

5.7 Total Mass and Energy Conservation in Calculations

Total mass conservation was very good (see Fig.11). About 1 to 2 g of mass was lost during the calculations. the deviation from mass conservation was less than 2 g in all calculations whereas the mass of the vapor field alone is 95 g (in 10 MPa experiments) and 290 g (in 2.14 MPa experiments). The standard SIMMER-II energy balance exhibited an error which was of the same order of magnitude as the calculated kinetic energy or was even higher (see Fig.12). As is shown in chapter 6, this error was closely correlated to the numerical loss of gas mass and it seemed that it had no direct relation to the accuracy of kinetic energies. This conclusion was reached in another context also in [12].

5.8 Influence of Dip Plate on Results

Table VIII summarises the effects of inserting the 20% (nominally; 32% virtually) open dip plate on important variables in experiments and calculations. As explained earlier (see Ch.4.6) the porosity of the dip plate had to be increased to give correct mass flow rates in benchmark problems (25% increase for the dip plate under investigation). To simulate the irreversible pressure losses at the dip plate the SIMMER-II orifice model was used with an appropriately adapted orifice coefficient. However, this pressure loss had a very small influence on the time development of the expansion. This was a surprise and could not be explained until we looked more closely to the flow behind the plate.

In all cases we found that very early in the expansion numerical cavitation effects developed in the pure liquid meshes directly above the dip plate. The cavitation started with very low pressures and a rapid build-up of high vapor volume fractions. The gas region increased and expanded in downstream direction. Liquid flowing out of the holes behind the dip plate could not mix with ambient fluid because there was little fluid left. Lacking other forces, this fluid then moved with high speed as an unimpeded liquid jet through the growing cavitation region until it met liquid at the end of the cavitation bubble. The flow resistance of the dip plate was therefore strongly determined by numerical cavitation effects and irreversible pressure losses played a

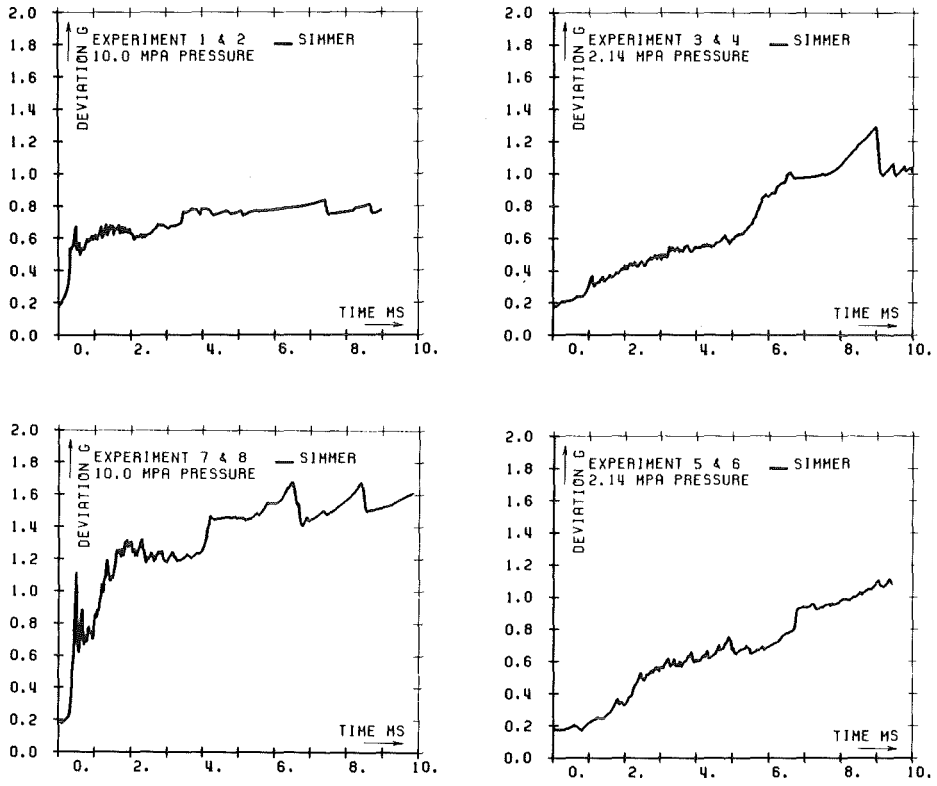

Figure 11: Total Mass Conservation in the Calculation

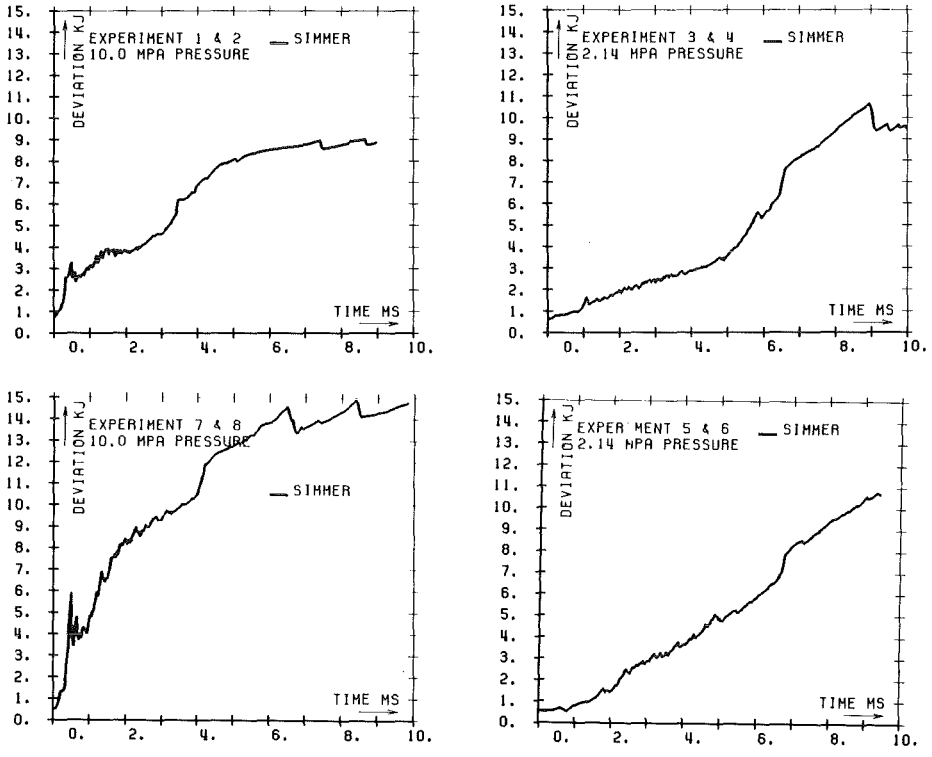

Figure 12: Total Energy Conservation in the Calculation

minor role.

In the experiments with the 10 MPa pressure source, the dip plate reduced kinetic energy (and energy conversion) by almost a factor of 3; impact pressures were reduced by a factor of 1.7. The calculations overestimated strongly the pressure reductions. Kinetic energy reduction on the other hand was underestimated by a factor of 2.

The experiments with the 2.14 MPa pressure source showed reductions in kinetic energy, impulses to the head, impact pressures and impact impulse of approximately a factor of 2; peak pressures decreased by 1.5 after insertion of the dip plate. In the calculations these reductions were greater for the impulse to the head and peak pressure but lower for kinetic energy, impact pressure and impact impulse.

Since bubble expansion and cover compression work had a good agreement in experiments and calculations, the energy conversion factors clearly reflected the differences in the determination of kinetic energies.

To summarise, SIMMER-II results for the calculations with and without dip plate displayed the same trend as indicated by the experiments. The reason for deviations (e.g. in kinetic energy and pressures) have been explained in the previous chapters.

5.9 Summary of Results

SIMMER-II hydrodynamics qualitatively reproduced the transient two-phase flow of the experiments quite well. Generally, the integral data showed satisfactory or good agreement. The code overestimated the development of kinetic energies because important dissipative processes (like vortices) are presently not modelled in it. This is especially pronounced for the dip plate experiments. Some difficulties showed up with local values like pressure values (spikes). Here numerical diffusion effects prevented an accurate treatment. SIMMER-II results for the calculations with and without dip plate showed the same trends as indicated by the experiments, but for a few of the variables this trend was strongly overestimated or underestimated. As explained earlier, this was due to numerical cavitation phenomena behind the dip plate and has to be investigated more closely in the near future.

TABLE VIII: Influence of Dip Plate on Results

Source Pressure	MPa	10.0	2.14
Impact Time[1]	ms		
Experiment		3.32/3.86/0.86	5.24/6.30/0.83
SIMMER-II Prediction		3.13/3.87/0.81	5.36/6.58/0.81
Impact Pressure[1]	MPa		
Experiment		34 / 20 /1.70	20 / 10 /2.00
SIMMER-II Prediction		15 / 4 /3.75	8 / 5 /1.60
Impact Impulse[1],[2]	kN*ms		
Experiment		157 /143 /1.10	207 /108 /1.92
SIMMER-II Prediction		135 / 97 /1.39	110 / 67 /1.64
Peak Pressure	MPa		
Experiment		34 / 35 /0.97	20 / 13 /1.54
SIMMER-II Prediction		23 / 8 /2.88	22 / 12 /1.83
Impulse to the Head[1]	kN*ms	t=9.0 ms	t=9.0 ms
Experiment		798 /456 /1.75	611 /293 /2.09
SIMMER-II Prediction		553 /440 /1.26	524 /232 /2.26
Expansion (displaced) Volume	ccm	t=1.9 ms	t=3.3 ms
Experiment		1346/ 924/1.46	1213/1132/1.07
SIMMER-II Prediction		1444/1143/1.26	1188/1033/1.15
Kinetic Energy of Liquid	KJ	t=1.9 ms	t=3.3 ms
Experiment		4.5 /1.6 /2.81	1.7 /0.9 /1.89
SIMMER-II Prediction		4.8 /3.4 /1.41	1.6 /1.2 /1.33
Bubble Expansion Work	KJ	t=1.9 ms	t=3.3 ms
Experiment		6.4 /5.4 / 1.2	2.6 /2.4 / 1.1
SIMMER-II Prediction		6.6 /6.0 / 1.1	2.5 /2.2 / 1.1
Cover Gas Compression Work	KJ	t=1.9 ms	t=3.3 ms
Experiment		0.2 /0.1 / 2.	0.1 /0.1 / 1.
SIMMER-II Prediction		0.2 /0.1 / 2.	0.1 /0.1 / 1.
Energy Conversion	%	t=1.9 ms	t=3.3 ms
Experiment		71 / 29 / 2.4	69 / 38 / 1.8
SIMMER-II Prediction		73 / 59 / 1.2	68 / 58 / 1.2

[1]: Quantities refer to the cover head (not to the dip plate).
[2]: This is defined as in Table VI.

Results are given in the form: a / b / c, where "a" is the value without, "b" the value with inserted dip plate and "c" the ration of both.

6.PARAMETER STUDIES AND SENSITIVITY ANALYSIS

The influence of some input variables had been studied: mesh size, maximum time step (variable DTMAX), tightening liquid gas coupling (parameter PIEE) and the single phase/two phase transition threshold (variable ALPHA0). These calculations were performed in a simplified model of the experimental apparatus; especially the dimensions of the different parts of the experiment were modified in such a way as to allow for a uniform mesh step axially and radially.

6.1 Influence of the Mesh Step Size

Calculations with uniform mesh sizes of 1, 2, 4 cm had been performed; the 1 cm calculation was considered to be the reference calculation for the following comparison.

Coarsening the mesh size shifted impact to later times (from 3.6 to 4.0 ms). This effect is due to the definition of impact time as the first pressure peak in the top central pressure transducer, because the pressure peak flattened out as the mesh size increases (see Fig.13). The general trend of all pressure curves was reproduced in all calculations (with some time delay and some broadening). Except for the time delay mentioned above, all impulse traces and the total impulse behaved in much the same way (deviations below 15%). Peak pressure was very sensitive to mesh refining as was to be expected (see the above discussion on numerical diffusion). A factor of 10 was between the 1 cm mesh and the 4 cm mesh.

The only effect of mesh size on displaced volumes was to determine the time at which bubble and cover gas region combined (at that time the evaluation of volumes broke down). The coarser the size, the earlier this combination took place.

Finer mesh sizes resulted in a somewhat higher (approximately 10%) peak kinetic energy. Bubble expansion work and cover compression work agreed very well.

In all calculations we had a clear correlation between total mass and total energy conservation (see Fig.14). Decreasing the spatial mesh

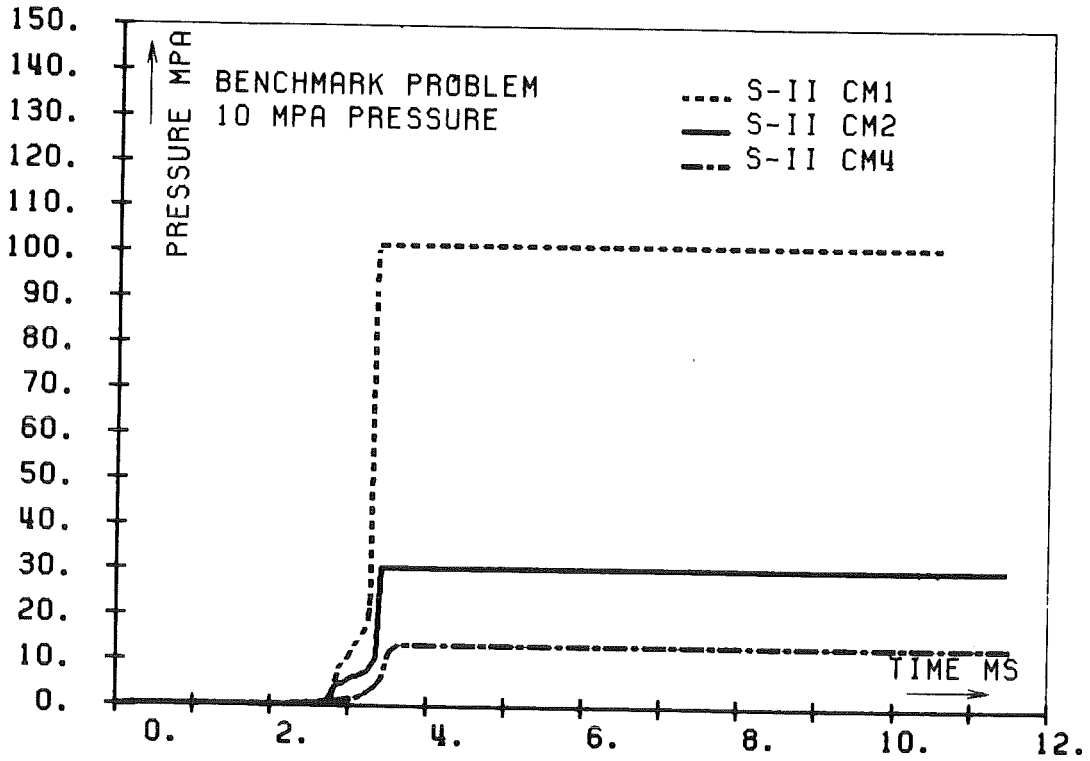

Figure 13: Influence of Mesh Size on Peak Pressures

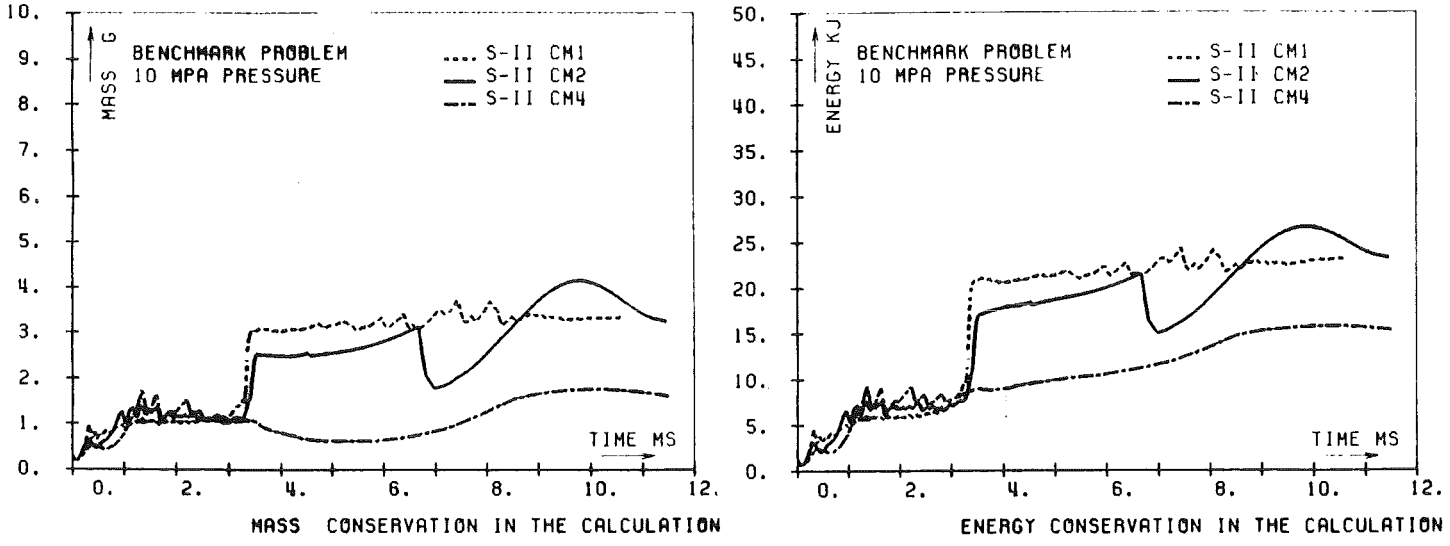

Figure 14: Correlation Between Total Mass and Total Energy Conservation

step size improved the conservation in the early phase (up to slug impact), though the results of all calculations were close together. For later times the the influence of mesh step size was just inverse. The reason for that was that the bigger mesh cells in the cover region were less prone to get into single-phase state. The transition from two-phase into single-phase obviously caused a loss of vapor mass and thereby of internal energy.

The deviation in energy conservation was about 5 - 10 KJ in the early phase and up to 25 KJ in the later times. This had to be compared with kinetic energies of up to 7 KJ (early phase) and 2 KJ (later phase). This comparison and the correlation mentioned above made us believe that the energy balance deviations could not serve as a good measure for the accuracy of the kinetic energy. This conjecture is corrobated by another investigation [12] where it was shown (in another context) that the kinetic energy was accurate to 1% while deviation from total energy conservation was an order of magnitude larger. We had evaluated the expression "Kinetic Energy + Cover Gas Compression Work - Bubble Expansion Work" for that purpose. Here the values rose from 0.0 to -2.5 KJ at 2 ms which was a factor 2 lower than kinetic energy.

From the above discussion follows that a mesh spacing of at least 1 cm is neccessary to reproduce impact time and pressure accurately enough (unfortunately, finer mesh steps are presently not possible because of memory and computing time limitations).

All calculations which are reported in the following were performed using the 2 cm mesh in order to save effort (even though some expected effects - see 6.4 - could not be observed with such a coarse mesh).

6.2 Influence of the Maximum Time Step Size

A test calculation has been performed with dtmax=1.0E-6 (in the standard calculations SIMMER-II choosed time steps between 1.0E-4 and 1.0E-5). The main influence was on peak pressures which increased from 30 to 48 MPa. This may be explained by the fact that the higher time resolution allowed to pick up more accurately the pressures at impact time. Note that computing times are very much higher with these fine time steps. The small effect of dtmax on all other variables confirmed that the SIMMER-II automatic time step control worked well in our case.

6.3 Influence of Changes in Liquid/Gas Coupling

The SIMMER-II liquid-vapor momentum exchange correlation contains a factor $\alpha_G^{-\lambda}$ ($\lambda>1$) to take account of the fact that the momentum exchange increases with increasing volume fraction of liquid. The standard calculations had been done with $\lambda=3.0$ (input variable PIEE). To investigate the influence of this (highly uncertain) constant additional calculations with $\lambda=1.0,5.0$ and 10.0 were done. The main effect of this variation: energy (and mass) conservation improved as λ decreased (from 27 to 20 KJ after the impact). The reason for this remains to be clarified, but it seems to be only a small effect. The expression "Kinetic Energy + Cover Compression Work - Bubble Expansion Work" was almost not affected by these variations.

6.4 Influence of the Single-Phase/Two-Phase Threshold

In SIMMER-II the input constant ALPHA0 is used to force a transition between single-phase and two-phase. Each mesh cell having a vapor volume fraction less than ALPHA0 is treated as single-phase whereas in the other case it is treated as two-phase. The standard calculations used a threshold of 0.02. To investigate the influence of this variable, we had varied ALPHA0 as: 0.001,0.01,0.05 and 0.10.

Impulse traces and total impulse to the head were little affected (but generally they were somewhat higher the lower the threshold). Kinetic energy was nearly identical for the time up to slug impact; only in the later phase some difference has been observed; but then the values of kinetic energy were more than a factor 3 smaller. Impact times were not affected by the variations of ALPHA0.

Energy (and mass) conservation improved considerably as ALPHA0 was decreased (from 10 KJ to 5KJ for the time up to impact; from 50 to 25 KJ for the following time). One would have expected that peak and impact pressures are strongly increased by reducing ALPHA0 (see [11]). No such effect has been observed since the mesh cell size (2 cm) was too large so that numerical diffusion prevented a noticeable effect of ALPHA0 on impact. Pressure oscillations for the time the bubble interface moved through the different positions were strongly influenced by the value of ALPHA0.

7.CALCULATIONAL PROBLEMS FOUND

Calculational problems found were:

(1) Numerical diffusion effects in SIMMER-II were observed (e.g., the bubble region coalesced with the cover gas very early; the amplitudes of the predicted impact pressures were too low);

(2) The expulsion predicted showed a certain time delay if compared with the experiment;

(3) SIMMER-II could not simulate high vorticity flow regions (e.g. behind the dip plate);

(4) The modelling of flow through perforated structures (like the dip plate) is still unsatisfactory mainly because of the numerical cavitation effects which could not be avoided;

(5) The SIMMER-II deviation from total energy conservation is not a valuable estimate for the accuracy of kinetic energies.

Issue (1) can be resolved at least partly by finer meshes, perhaps by appropriate criteria for the transition of single- to two-phase flow and improving the gas-liquid momentum coupling.

Issue (2) can only be improved by modifying the numerical schemes of SIMMER-II. Comparisons with the experiments showed that the emptying of the upper core in the calculation was too slow. This probably can be attributed to the momentum calculation when the water was accelerated initially and expelled from the upper core into the pool area. For the comparisons between SIMMER-II and experimental results presented here, this point was of minor importance during the early expansion phase because these inaccuracies had been eliminated by the special synchronisation scheme.

Issue (3) requires a better description of vorticity in SIMMER-II. As it may be expected that a full account of vortices in a code of this size will not be practical, a cruder method (e.g. using the general mixing characteristics behind the dip plate) should be investigated.

Issue (4) still needs further investigations about the conditions under which numerical cavitation occurs. Improvements of SIMMER-II seem also be neccessary for fluid flow at abrupt area changes.

Issue (5) could be resolved for the present applications by introducing the quantity "kinetic energy + cover gas compression work - bubble expansion work". This formula is, however, not generally usable.

Improvement is needed for the check of input data: the vast amount of input data to SIMMER-II contains some parts which are not independent of each other. There is some danger that contradictious or meaningless values are introduced, pass the present SIMMER-II input phase and lead to erroneous results and/or breakdown of the calculation. Often these difficulties are only recognised after the run, thus wasting computer time and evaluation effort. The development of a separate code or the inclusion of a subroutine in SIMMER-II which checks the input for consistency and plausibility might help considerably. In the long term, it would certainly be better to rewrite the input routine of SIMMER-II totally to eliminate redundant and - possibly - inconsistent input data.

8. CONCLUSIONS

Fluid dynamical experiments for the postdisassembly expansion phase in SNR-typical geometry have been investigated using the SIMMER-II code. The main goal of this investigation was to test whether the SIMMER-II code could reproduce the important experimental features during the expansion and the subsequent collapse of the high pressure gas bubble. Comparisons between the experimental and calculated results were concentrated on local pressures, impulses on various structures, displaced volumes and kinetic energies of the liquid.

To optimize the input parameters for the SIMMER-II calculations sensitivity studies were performed. After the input data were optimized with respect to the experimental geometry (mesh structure and size) and to other important fluid dynamics parameters (time step size, single phase/two phase threshold) SIMMER-II results agreed for the cases without dip plates quite well with the measured values for the important dynamical variables mentioned above. Numerical deficiencies found in these cases were: inaccuracies in the solution of the momentum equation in the early phase, when the water of the above core region was pushed into the pool; numerical diffusion problems which smeared out the gas/liquid interfaces and rendered impossible the accurate calculation of head impact pressures.

For the cases with dip plates additional numerical problems were found: the flow rates through the dip plates were too low and numerical cavitations behind the plates prevented the accurate calculation of the flow there. As a consequence the impact on the head was not well represented. These problems together with other modelling deficiencies (e.g. the vortex formation behind the dip plate) were responsible for rather inaccurate SIMMER-II results for the kinetic energy of the liquid and the pressure on the cover head. As would have been expected, the displaced volume calculations in the early development of the bubble were not strongly affected by the insertion of dip plates.

The results presented here agree generally with the outcome of similar SIMMER-II studies of the expansion phase done at Los Alamos [11]. A scaled CRBR vessel was used in that investigation and various

above core structures were systematically added to the basic configuration. The quality of SIMMER-II results decreased rapidly when complex internal structures were inserted into the vessel. Because other types of internals (like the dip plates) were used in our SNR-typical geometry, the weak points of SIMMER-II with respect to the flow representation in and near complicated perforated structures could be more easily pinned down in the study presented here.

It is our aim to concentrate in the near future on the neccessary improvements of SIMMER-II fluid-dynamics with respect to internal structures. It seems to be mandatory to implement these improvements into the code before experiments with more complicated internals (e.g. the upper core or upper internal structures) can be interpreted with the outcome of SIMMER-II simulations.

ACKNOWLEDGEMENTS

The authors would like to thank R.J.Tobin and A.L.Florence of SRI International for performing the experimental program. The help of R.Heger and S.Kleinheins (KfK/INR) with coding assistance and W.Maschek (KfK/INR) for helpful discussions is greatly acknowledged.

REFERENCES

[1] P.Royl et al.,"Untersuchungen zu Kühlmitteldurchsatzstörfällen im abgebrannten Mark IA-Kern des Kernkraftwerks Kalkar", Report KfK 2845, Karlsruhe (1979)

[2] L.L.Smith et al.,"SIMMER-II: A Computer Program for LMFBR Disrupted Core Analysis", Report NUREG/CR-0453; LA-7515-M (Rev.), Los Alamos (1980)

[3] R.J.Tobin, A.L.Florence,unpublished research report (1981)

[4] K.Küfner et al., "Model Experiments for the Postdisassembly Expansion Phase in LMFBRs and Their Use for Code Verification,", Proc. Int. Top. Meeting on LMFBR Safety, Lyon, France, p.IV-99 (1982)

[5] R.J.Tobin, D.J.Cagliostro, "Effects of Vessel Internal Structures on Simulated HCDA Bubble Expansions", Technical Report No. 5, DOE/SF/70097--T9, SRI International, Menlo Park, CA, USA (1978)

[6] P.E.Rexroth, A.J.Suo-Anttila, "SIMMER Analysis of SRI High Pressure Bubble Expansion Experiments", Proc. Specialists' Workshop on Predictive Analysis of Material Dynamics in LMFBR Safety Experiments, March 13-15, 1979, Los Alamos, NM, USA, M.G.Stevenson (comp.), LA-7938-C, p. 308-319 (1979)

[7] K.Küfner, P.Schmuck, R.Fröhlich, "SIMMER-II Calculations for Simulation Experiments of the Postdisassembly Expansion Phase in an ULOF Accident," Proc. Jahrestagung Kerntechnik 1983, Berlin, Germany (1983) S. 129

[8] P.Schmuck, in "Multiphase Processes in LMFBR Safety Analysis," (A.V.Jones, Ed.), Harwood Academic Publishers, London/Paris, p.431 (1984)

[9] P.Schmuck, personal communication (March 1983)

[10] ref.[3], supplementary volume

[11] T.F.Bott, C.R.Bell, "SIMMER-II Analysis of SRI Postdisassembly Expansion Phase," Report LA-9452-MS, Los Alamos, N.M., (1982)

[12] P.Schmuck, "A Study of Some Numerical Problems for SIMMER-II Fluid-Dynamics," Report KfK 3284, Karlsruhe (1982)

APPENDIX A: TYPICAL SIMMER-II INPUT DATA

The following pages contain typical SIMMER-II input parameters used for the presented analyses. More specific: this input was used for the analysis of the 10 MPa experiment with an inserted dip plate (experiment no. 7).

NUMERICAL METHODS PARAMETERS-

COMPRESSIBLE EPSILON-1	(EPS)=	0.10000D-03
COMPRESSIBLE EPSILON-2	(EPC)=	0.10000D-05
INCOMPRESSIBLE EPSILON-1	(EPIR)=	0.10000D-03
INCOMPRESSIBLE EPSILON-2	(EPI)=	0.10000D-02
VAPOR VOLUME FRACTION FOR SINGLE/TWO-PHASE TRANSITION	(ALPHO)=	0.20000D-01
PROPORTION OF DONOR CELL WEIGHTING TO BE USED	(AO)=	0.50000D+00
THE AMOUNT OF CONVECTIVE FLUXING TO BE USED	(BO)=	0.0
OPTIMUM NUMBER OF PRESSURE ITERATIONS	(ITOPT)=	4
MAXIMUM NUMBER OF PRESSURE ITERATIONS ALLOWED	(NITMAX)=	100
MAXIMUM NUMBER OF MATRIX SOLUTION ITERATIONS ALLOWED IN MATSOL	(MITMAX)=	500
NUMBER OF MATSOL ITERATIONS TO TEST ROW AND COLUMN LINE INVERSION	(MITCRC)=	50
MINIMUM NUMBER OF TIME STEPS BETWEEN TESTING ROW AND COLUMN INVERT	(NITCRC)=	20
NUMBER OF MATSOL ITERATIONS BETWEEN SPECTRAL RADIUS UPDATES	(NITSRU)=	5
THE INNER ITERATION PHASE EPSILON	(EPHASE)=	1.00000D-08
THE EPSILON FOR THE VAPOR ENERGY EQUATION	(EVAPOR)=	5.00000D-02
PRESSURE CONVERGENCE EPSILON	(EPSP)=	0.10000D-11
LIQUID COMPONENT DENSITY CONVERGENCE EPSILON	(EPSL)=	0.10000D-11
VAPOR COMPONENT DENSITY CONVERGENCE EPSILON	(EPSV)=	0.10000D-11
VAPOR CUTOFF DENSITY	(ROGCUT)=	0.10000D-04

TIME STEP CONTROLS-

STARTING TIME	(T)=	0.35000D-02
INITIAL TIME STEP	(DTSTAR)=	0.10000D-04
NUMBER OF CYCLES TO HOLD DTSTAR	(NDTO)=	5
THE MINIMUM TIME STEP ALLOWED	(DTMIN)=	0.10000D-08
THE MAXIMUM TIME STEP ALLOWED	(DTMAX)=	0.10000D-02
COURANT CONDITION PARAMETER	(COURNT)=	0.13000D+00
FRACTIONAL VAPOR DENSITY CHANGE FOR CONDENSATION PER TIME STEP	(DJMAX)=	0.50000D+00
FRACTIONAL VAPOR DENSITY CHANGE FOR VAPORIZATION PER TIME STEP	(DROJAY)=	0.10000D+01
ENERGY DENSITY CHANGE ALLOWED IN A TIME STEP	(DTMPM)=	0.10000D+02
MAXIMUM FRACTIONAL CHANGE IN REACTIVITY DURING A TIME STEP	(DREAMX)=	0.10000D+01
MAXIMUM FRACTIONAL CHANGE IN THE POWER DURING A TIME STEP	(DPOWMX)=	0.10000D+01

STRUCTURE FAILURE PARAMETERS-

MAXIMUM STRUCTURE MACRO DENSITY ALLOWED TO FAIL EACH TIME STEP	(ROSMLT)=	1.00000D+02
MINIMUM INTACT CLAD MACRO DENSITY	(RSCLAD)=	1.00000D+00
MINIMUM INTACT SUBASSEMBLY CAN WALL MACRO DENSITY	(ROSFAL)=	1.00000D+00
RADIAL MOTION RESTRAINT CONDITION INDICATOR	(IFGFAL)=	0

STRUCTURE AND SOLID MATERIAL FAILURE PARAMETERS

STRUCTURE AND SOLID MATERIAL	N	FRACTION OF HEAT OF FUSION ABOVE SOLIDUS ENERGY DEFINING FAILURE ENERGY FFLR(N)	FRACTION OF MELTED MATERIAL THAT IS LIQUID XFLR(N)
FABRICATED FUEL	1	0.90000D+00	0.10000D+01
REFROZEN FUEL	2	0.90000D+00	0.10000D+01
STEEL CLADDING	3	0.50000D+00	0.51000D+00
STEEL CAN WALL	4	0.50000D+00	0.10000D+01
CONTROL	5	0.0	
FUEL PARTICLES	6	0.0	
STEEL PARTICLES	7	0.0	

MAXIMUM MASS TRANSFER RATE OF FAILED STRUCTURE TO THE LIQUID/VAPOR FIELD

STRUCTURE MATERIAL	N	RFLR(N)	STRUCTURE MATERIAL	N	BEFORE CLAD FAILURE CFLR(N)
FABRICATED FUEL	1	0.30000D+07	FABRICATED FUEL	1	0.30000D+05
REFROZEN FUEL	2	0.10000D+07	CONTROL	2	0.90000D+04
CLADDING	3	0.70000D+06	INTERGRANULAR FISSION GAS	3	0.20000D+02
CAN WALL	4	0.80000D+06			
CONTROL	5	0.90000D+06			
INTERGRANULAR FISSION GAS	6	0.20000D+04			

MATERIAL PROPERTIES AND EQUATION OF STATE DATA

		FUEL (not used)	STEEL (& acryl)	SODIUM (water)	CONTROL (not used)	FISSION GAS (nitrogen)
---------SOLID STATE----------						
MICROSCOPIC DENSITY	ROSE	9.89000D+03	7.36500D+03	5.00000D+02	2.52000D+03	0.0
SPECIFIC HEAT	CVS	6.38000D+02	6.39000D+02	2.09000D+03	1.89300D+03	0.0
MELT TEMPERATURE	TMLT	3.10000D+03	1.70000D+03	2.73160D+02	2.62300D+03	0.0
HEAT OF FUSION	HFUS	2.76000D+05	2.60000D+05	3.33400D+05	2.50000D+05	0.0
THERMAL CONDUCTIVITY	THCONS	2.00000D+00	2.50000D+01	6.80000D-01	8.37400D+01	0.0
---------LIQUID STATE----------						
MICROSCOPIC DENSITY	ROLE	8.58000D+03	6.10000D+03	1.00178D+03	2.52000D+03	0.0
SPECIFIC HEAT	CVL	5.04000D+02	7.50000D+02	4.21710D+03	1.89000D+03	0.0
SURFACE TENSION	SIG	4.50000D-01	1.60000D+00	7.27000D-02	1.00000D+00	0.0
THERMAL CONDUCTIVITY	THCONL	2.50000D+00	2.00000D+01	6.80000D-01	8.00000D+01	0.0
VISCOSITY	XMUL	4.30000D-03	5.36000D-03	1.00000D-04	1.00000D-03	0.0
---------VAPOR STATE----------						
VAPOR PRESSURE PARAMETER	PSTAR	1.44000D+11	1.33800D+11	3.17771D+10	4.28600D+14	1.00000D+11
VAPOR PRESSURE PARAMETER	TSTAR	5.17080D+04	4.33700D+04	4.70579D+03	8.36800D+04	4.00000D+04
SUPERHEAT	TSUP	0.0	0.0	0.0	0.0	0.0
HEAT OF VAPORIZATION PARAMETER	HSTAR	2.62000D+06	8.17000D+06	3.22689D+06	5.00000D+06	5.00000D+06
CRITICAL TEMPERATURE	TCRIT	8.40000D+03	1.00000D+04	6.47286D+02	7.10700D+03	1.26200D+02
HEAT OF VAPORIZATION PARAMETER	ZETA	5.97000D-01	3.60000D-01	3.90597D-01	3.50000D-01	3.00000D-01
SPECIFIC HEAT	CVG	5.11000D+02	4.92000D+02	1.40200D+03	5.00000D+02	7.27000D+02
SPECIFIC HEAT RATIO	GAM	1.05000D+00	1.26000D+00	1.32900D+00	1.50000D+00	1.40400D+00
MOLECULAR DIAMETER	ATOM	4.40000D+00	1.64000D+00	3.73700D+00	1.46000D+00	3.79800D+00
CRITICAL ENERGY	ENCRIT	4.92500D+06	8.17000D+06	2.93390D+06	1.36901D+07	5.00000D+06
MOLECULAR WEIGHT	WTMOL	2.70000D+02	5.60000D+01	1.80000D+01	5.53000D+01	2.80130D+01
MOLECULAR FORCE CONSTANT	EPSK	6.46800D+03	7.70000D+03	3.20000D+01	5.47200D+03	7.14000D+01
POLY-ATOMIC FLAG	MONO	1	1	1	1	1

LIQUID AND SOLID COMPONENT PROPERTIES

COMPONENT NUMBER N	SOLID MICROSCOPIC DENSITY ROS(N)	LIQUID MICROSCOPIC DENSITY ROL(N)	LIQUID SONIC VELOCITY SVEL(N)
1	0.98900D+04	0.85800D+04	0.20000D+04
2	0.98900D+04	0.85800D+04	0.20000D+04
3	0.98900D+04	0.61000D+04	0.20000D+04
4	0.98900D+04	0.10000D+04	0.15000D+04
5	0.73650D+04	0.25200D+04	0.20000D+04
6	0.73650D+04	0.98900D+04	0.20000D+04
7	0.25200D+04	0.98900D+04	0.20000D+04
8	0.0	0.73650D+04	0.20000D+04
9	0.0		

ENERGY EXCHANGE FUNCTION PARAMETERS

HEAT TRANSFER CORRELATION COEFFICIENTS

LIQUID FUEL-STRUCTURE CORRELATION	NU= 0.23000D-01*(RE** 0.80000D+00)*(PR** 0.40000D+00)+ 0.0
LIQUID STEEL-STRUCTURE CORRELATION	NU= 0.25000D-01*(RE** 0.80000D+00)*(PR** 0.80000D+00)+ 0.50000D+01
LIQUID SODIUM-STRUCTURE CORRELATION	NU= 0.10000D-09*(RE** 0.80000D+00)*(PR** 0.40000D+00)+ 0.0
LIQUID CONTROL-STRUCTURE CORRELATION	NU= 0.23000D-01*(RE** 0.80000D+00)*(PR** 0.40000D+00)+ 0.0
VAPOR-STRUCTURE CORRELATION	NU= 0.10000D-09*(RE** 0.80000D+00)*(PR** 0.40000D+00)+ 0.0
LIQUID-VAPOR CORRELATION	NU= 0.10000D-09*(RE** 0.80000D+00)*(PR** 0.40000D+00)+ 0.0

LIQUID-LIQUID HEAT TRANSFER MULTIPLIER MATRIX

	LIQUID STEEL	LIQUID SODIUM	LIQUID CONTROL	SOLID FUEL	SOLID STEEL
LIQUID FUEL	0.0	0.0	0.0	0.0	0.0
LIQUID STEEL		0.0	0.0	0.0	0.0
LIQUID SODIUM			0.0	0.0	0.0
LIQUID CONTROL				0.0	0.0
SOLID FUEL					0.0

MOMENTUM EXCHANGE FUNCTION PARAMETERS

DRAG CORRELATION COEFFICIENTS

LIQUID-STRUCTURE TURBULENT CORRELATION	F=	0.46000D-01*RE**-0.20000D+00
MINIMUM LIQUID-STRUCTURE FRICTION FACTOR	(FRLMIN)=	0.10000D-02
VAPOR-STRUCTURE TURBULENT CORRELATION	F=	0.46000D-01*RE**-0.20000D+00
MINIMUM VAPOR-STRUCTURE FRICTION FACTOR	(FRGMIN)=	0.10000D-02
ORIFICE COEFFICIENT INPUT INDICATOR	(IORCO)=	1
AXIAL LOCATION OF ORIFICE	(LOCORF)=	25
STR.VOL.FR.ABOVE WHICH DRAG IS INFINITE	(ALDRG)=	0.90000D+00
VAPOR KINEMATIC VISCOSITY	(FNUG)=	0.20000D-03
LIQUID KINEMATIC VISCOSITY	(FNUL)=	0.92000D-06
LIQUID-VAPOR DRAG COEFFICIENT	(CDR)=	0.10000D+01
CRITICAL WEBER NUMBER	(WEBCRT)=	0.22000D+02
VISCOSITY INDICATOR	(IVIS)=	1
COALESCENCE PARAMETER	(COAL)=	0.10000D+01
PARTICLE INTERFERENCE EFFECT EXPONENT	(PIEE)=	0.30000D+01
DROPLET SIZE DISTRIBUTION MULTIPLIER	(DSDM)=	0.10000D+01
TWO PHASE WEIGHTING FACTOR	(TPWF)=	0.50000D+00
PARTICLE VISCOSITY COEFFICIENT	(PARVIS)=	1.00000D+00
MAXIMUM PACKING FRACTION	(PKFMAX)=	4.00000D-01
PHASE TRANSITION MODEL RATE CONSTANT	(TIMCT)=	1.00000D+00

MASS EXCHANGE FUNCTION PARAMETERS

VAPOR VOLUME FRACTION BELOW WHICH VAPOR CONDENSATION ON THE STRUCTURE DOES NOT OCCUR	(ALCSCO)=	0.50000D+00
STRUCTURE CONDENSATION RATE COEFFICIENT	(SCRC)=	0.10000D+01
AEOS CONVERGENCE PARAMETER	(CAEOS)=	0.10000D-09

PARAMETER REGION INPUT-

NUMBER OF PARAMETER REGIONS (NPAREG)= 6

		PARAMETER REGION NUMBER				
		1 (nitrogen)	2 (structures)	3 (cover gas)	4 (water)	5 (sliding doors)
MESH CELL INDICATOR	RGTYP	0.70000D+01	0.50000D+01	0.70000D+01	0.70000D+01	0.70000D+01
NONFLOW VOLUME FRACTION	ALNOFL	0.0	0.0	0.0	0.0	0.0
NONFLOW PRESSURE	PNOFL	0.10000D+06	0.10000D+06	0.10000D+06	0.10000D+06	0.10000D+06
PELLET RADIUS	RPELL	0.0	0.0	0.0	0.0	0.0
CLADDING RADIUS	RCLAD	0.0	0.0	0.0	0.0	0.0
CAN WALL THICKNESS	THCANW	0.10000D-04	0.25000D-02	0.10000D-04	0.10000D-04	0.10000D-04
PELLET SURFACE AREA	APELL	0.0	0.0	0.0	0.0	0.0
CLADDING SURFACE AREA	ACLAD	0.0	0.0	0.0	0.0	0.0
CAN WALL SURFACE AREA	ACAN	0.10000D-03	0.10000D+01	0.10000D-03	0.10000D-03	0.10000D-03
PELLET VOLUME FRACTION	VFPELL	0.0	0.0	0.0	0.0	0.0
CLADDING VOLUME FRACTION	VFCLAD	0.0	0.87004D+00	0.0	0.0	0.0
CAN WALL VOLUME FRACTION	VFCANW	0.0	0.11000D+00	0.0	0.0	0.0
INTACT GEO. HYDR. DIA.	DHINGE	0.10000D+03	0.12500D-02	0.10000D+03	0.10000D+03	0.10000D+03
NO CLAD HYDR. DIA.	DHNCLD	0.10000D+03	0.12500D-02	0.10000D+03	0.10000D+03	0.10000D+03
NO PIN HYDR. DIA.	DHNPEL	0.10000D+03	0.12500D-02	0.10000D+03	0.10000D+03	0.10000D+03
PELLET HEAT TRAN. COEF.	HTCPEL	0.0	0.17900D+05	0.0	0.0	0.0
CLADDING HEAT TRAN. COEF.	HTCCLD	0.0	0.17900D+05	0.0	0.0	0.0
CAN WALL HEAT TRAN. COEF.	HTCCAN	0.10000D-04	0.50000D+03	0.10000D-04	0.10000D-04	0.10000D-04
STEADY STATE FUEL TEMPERATURE	TSSF	2.93000D+02	2.93000D+02	2.93000D+02	2.93000D+02	2.93000D+02
UNRESTRUCTURED FUEL FRACTION	FURSF	9.00000D-01	9.00000D-01	9.00000D-01	9.00000D-01	9.00000D-01
PRESS.DIFF.ACROSS UNRESTR.FUEL	DPURSF	0.0	1.00000D+05	0.0	0.0	0.0
FUEL GRAIN RADIUS	RGRAIN	0.0	2.30000D-05	0.0	0.0	0.0
FUEL PERMEABILITY	PERMF	0.0	1.00000D-17	0.0	0.0	0.0
MAXIMUM DROPLET RADIUS	RPMAX	1.00000D-03	1.00000D-03	1.00000D-03	1.00000D-03	1.00000D-03
MINIMUM DROPLET RADIUS	RPMIN	1.00000D-05	1.00000D-05	1.00000D-05	1.00000D-05	1.00000D-05
SATURATED GRAIN GAS DENSITY	RHOSAT	0.0	0.0	0.0	0.0	0.0
CAN WALL NO FLOW VOLUME FRACTION	ALNFCW	0.0	0.0	0.0	0.0	0.0

		PARAMETER REGION NUMBER
		6 (dip plate)
MESH CELL INDICATOR	RGTYP	0.50000D+01
NONFLOW VOLUME FRACTION	ALNOFL	0.0
NONFLOW PRESSURE	PNOFL	0.10000D+06
PELLET RADIUS	RPELL	0.0
CLADDING RADIUS	RCLAD	0.0
CAN WALL THICKNESS	THCANW	0.10000D+00
PELLET SURFACE AREA	APELL	0.0
CLADDING SURFACE AREA	ACLAD	0.10000D+01
CAN WALL SURFACE AREA	ACAN	0.10000D+01
PELLET VOLUME FRACTION	VFPELL	0.0
CLADDING VOLUME FRACTION	VFCLAD	0.10000D-01
CAN WALL VOLUME FRACTION	VFCANW	0.10000D-02
INTACT GEO. HYDR. DIA.	DHINGE	0.10000D+03
NO CLAD HYDR. DIA.	DHNCLD	0.10000D+03
NO PIN HYDR. DIA.	DHNPEL	0.10000D+03
PELLET HEAT TRAN. COEF.	HTCPEL	0.0
CLADDING HEAT TRAN. COEF.	HTCCLD	0.10000D-09
CAN WALL HEAT TRAN. COEF.	HTCCAN	0.50000D+03
STEADY STATE FUEL TEMPERATURE	TSSF	2.93000D+02
UNRESTRUCTURED FUEL FRACTION	FURSF	6.80000D-01
PRESS.DIFF.ACROSS UNRESTR.FUEL	DPURSF	1.00000D+03
FUEL GRAIN RADIUS	RGRAIN	2.30000D-05
FUEL PERMEABILITY	PERMF	1.00000D-17
MAXIMUM DROPLET RADIUS	RPMAX	1.00000D-03
MINIMUM DROPLET RADIUS	RPMIN	1.00000D-05
SATURATED GRAIN GAS DENSITY	RHOSAT	0.0
CAN WALL NO FLOW VOLUME FRACTION	ALNFCW	0.60000D+00

BOUNDARY CONDITIONS-

BOUNDARY CONDITION INDICATOR FOR THE ENTIRE BOTTOM BOUNDARY (IBOT)= 0
BOUNDARY CONDITION INDICATOR FOR THE ENTIRE TOP BOUNDARY (ITOP)= 0

THE LOWER BOUNDARY IS RIGID FOR THIS CASE
THE TOP BOUNDARY IS RIGID FOR THIS CASE

BOUNDARY CONDITION INDICATOR FOR THE RIGHT DOUNDARY ABOVE JRIGID (IRIGHT)= 0

NOMINAL RIGHT HAND SIDE BOUNDARY CONDITIONS APPLY TO THIS CASE
0.0 0.0

THE NUMBER OF CELLS ON THE RIGHT BOUNDARY WHICH ARE RIGID (JRIGID)= 41

********** VAPOR AND LIQUID VELOCITIES ON THE BOTTOM BOUNDARY *****

VAPOR AXIAL VELOCITY AT THE BOTTOM BOUNDARY (VG(I))=	0.0	0.0	0.0	0.0	0.0
	0.0	0.0	0.0	0.0	0.0
	0.0	0.0	0.0	0.0	0.0
	0.0	0.0	0.0	0.0	
LIQUID AXIAL VELOCITY AT THE BOTTOM BOUNDARY (VL(I))=	0.0	0.0	0.0	0.0	0.0
	0.0	0.0	0.0	0.0	0.0
	0.0	0.0	0.0	0.0	0.0
	0.0	0.0	0.0	0.0	

ADDITIONAL INFORMATION FOR THE AEOS

		FUEL	STEEL	SODIUM	CONTROL	FISSION GAS
CRITICAL PRESSURE	PCRIT	3.05471D+08	1.74953D+09	2.21197D+07	3.30016D+09	0.0
CRITICAL DENSITY	ROGCRT	3.21750D+03	2.28750D+03	3.16957D+02	9.45000D+02	0.0
DENSITY AT TSAT=.95*TCRIT	ROGP95	1.08361D+03	1.14584D+03	9.57700D+01	1.05209D+03	0.0
CONST PART OF LIQUID HEAT CAPACITY	CVLP	2.61187D+02	1.04428D+02	1.44265D+03	1.17157D+03	7.27000D+02
PARAMETER IN LIQUID ENERGY EQN	AEOSLM	1.93988D+06	6.47561D+06	1.71833D+06	5.69930D+06	4.96942D+06
FITTING PARAMETER A10 FOR R	AEOS10	3.24064D+00	4.85141D+00	6.13401D+00	5.52146D+00	0.0
FITTING PARAMETER A20 FOR R	AEOS20	0.0	-1.92865D-17	3.83207D-06	1.92865D-17	0.0
FITTING PARAMETER A30 FOR R	AEOS30	0.0	2.69200D-19	-2.42361D-03	-9.16434D-19	0.0
FITTING PARAMETER A11 FOR R	AEOS11	4.14354D+00	5.23538D+00	6.38815D+00	-7.57811D+02	0.0
FITTING PARAMETER A21 FOR R	AEOS21	-2.76423D-04	4.25199D-05	-3.12498D-03	5.90387D-01	0.0
FITTING PARAMETER A31 FOR R	AEOS31	-1.04145D-08	-4.81610D-08	-1.42460D-06	-1.14055D-04	0.0

INPUT FOR MESH POINT SET 1

MESH POINT SET DESCRIPTION ****** MESH CELL SET 1 : INITIALISATION WITH WATER *********

MESH POINT SET BOUNDARIES BOTTOM (NB)= 1 TOP (NT)= 41 LEFT (NL)= 1 RIGHT (NR)= 19
IINP= 1 VAPOR DENSITIES AND TEMPERATURE INPUT--VAPOR PRESSURE DETERMINED
ISAT= 0 LIQUID TEMPERATURE DETERMINED BY INPUT DATA
IPAREG= 4 PARAMETER REGION NUMBER
ICELWS= 0 NUMBER OF COMPOSITION PARAMETERS TO HAVE THEIR VALUES INPUT MESH CELLWISE

MESH POINT SET DENSITIES AND TEMPERATURES

COMPONENT NUMBER N	STRUCTURE MACROSCOPIC DENSITY RSBRI(N)	STRUCTURE TEMPERATURE TSI(N)	LIQUID MACROSCOPIC DENSITY RLBRI(N)	LIQUID TEMPERATURE TLI(N)	VAPOR MICROSCOPIC DENSITY ROGI(N)
1	0.0	0.29300D+03	0.0	0.29300D+03	0.0
2	0.0	0.29300D+03	0.0	0.29300D+03	0.0
3	0.0	0.29300D+03	0.0	0.29300D+03	0.0
4	0.0	0.29300D+03	0.98000D+03	0.29300D+03	0.73993D+00
5	0.0	0.29300D+03	0.0	0.29300D+03	0.0
6	0.0		0.0	0.29300D+03	0.0
7	0.0		0.0		
8	0.0		0.0		
9	0.0				

VAPOR STATE	TEMPERATURE	TGI= 0.29300D+03	PRESSURE	PNI= 0.0
AXIAL VELOCITIES	VAPOR	VGI= 0.0	LIQUID	VLI= 0.0
RADIAL VELOCITIES	VAPOR	UGI= 0.0	LIQUID	ULI= 0.0
SOLID PARTICLE RADII	FUEL	RPSFI= 0.50000D-05	STEEL	RPSSI= 0.50000D-04

INPUT FOR MESH POINT SET 2

MESH POINT SET DESCRIPTION ****** MESH CELL SET 2 : PRESSURE SOURCE 1 **********

MESH POINT SET BOUNDARIES BOTTOM (NB)= 1 TOP (NT)= 5 LEFT (NL)= 1 RIGHT (NR)= 5
IINP= 1 VAPOR DENSITIES AND TEMPERATURE INPUT--VAPOR PRESSURE DETERMINED
ISAT= 0 LIQUID TEMPERATURE DETERMINED BY INPUT DATA
IPAREG= 1 PARAMETER REGION NUMBER
ICELWS= 0 NUMBER OF COMPOSITION PARAMETERS TO HAVE THEIR VALUES INPUT MESH CELLWISE

MESH POINT SET DENSITIES AND TEMPERATURES

COMPONENT NUMBER N	STRUCTURE MACROSCOPIC DENSITY RSBRI(N)	STRUCTURE TEMPERATURE TSI(N)	LIQUID MACROSCOPIC DENSITY RLBRI(N)	LIQUID TEMPERATURE TLI(N)	VAPOR MICROSCOPIC DENSITY ROGI(N)
1	0.0	0.29300D+03	0.0	0.29300D+03	0.0
2	0.0	0.29300D+03	0.0	0.29300D+03	0.0
3	0.0	0.29300D+03	0.0	0.29300D+03	0.0
4	0.0	0.29300D+03	0.99300D-01	0.29300D+03	0.78676D-03
5	0.0	0.29300D+03	0.0	0.29300D+03	0.0
6	0.0		0.0	0.29300D+03	0.11620D+03
7	0.0		0.0		
8	0.0		0.0		
9	0.0				

VAPOR STATE	TEMPERATURE	TGI= 0.29300D+03	PRESSURE	PNI= 0.0
AXIAL VELOCITIES	VAPOR	VGI= 0.0	LIQUID	VLI= 0.0
RADIAL VELOCITIES	VAPOR	UGI= 0.0	LIQUID	ULI= 0.0
SOLID PARTICLE RADII	FUEL	RPSFI= 0.50000D-05	STEEL	RPSSI= 0.50000D-04

INPUT FOR MESH POINT SET 3

MESH POINT SET DESCRIPTION ****** MESH CELL SET 3 : RIGID STRUCTURE 1 **********

MESH POINT SET BOUNDARIES BOTTOM (NB)= 1 TOP (NT)= 8 LEFT (NL)= 6 RIGHT (NR)= 19
IINP= 1 VAPOR DENSITIES AND TEMPERATURE INPUT--VAPOR PRESSURE DETERMINED
ISAT= 0 LIQUID TEMPERATURE DETERMINED BY INPUT DATA
IPAREG= 2 PARAMETER REGION NUMBER
ICELWS= 0 NUMBER OF COMPOSITION PARAMETERS TO HAVE THEIR VALUES INPUT MESH CELLWISE

MESH POINT SET DENSITIES AND TEMPERATURES

COMPONENT NUMBER N	STRUCTURE MACROSCOPIC DENSITY RSBRI(N)	STRUCTURE TEMPERATURE TSI(N)	LIQUID MACROSCOPIC DENSITY RLBRI(N)	LIQUID TEMPERATURE TLI(N)	VAPOR MICROSCOPIC DENSITY ROGI(N)
1	0.0	0.29300D+03	0.0	0.29300D+03	0.0
2	0.0	0.29300D+03	0.0	0.29300D+03	0.0
3	0.0	0.29300D+03	0.0	0.29300D+03	0.0
4	0.0	0.29300D+03	0.10000D+02	0.29300D+03	0.73993D+00
5	0.64075D+04	0.29300D+03	0.0	0.29300D+03	0.0
6	0.81015D+03		0.0	0.29300D+03	0.0
7	0.0		0.0		
8	0.0		0.0		
9	0.0				

VAPOR STATE	TEMPERATURE	TGI= 0.29300D+03	PRESSURE	PNI= 0.0
AXIAL VELOCITIES	VAPOR	VGI= 0.0	LIQUID	VLI= 0.0
RADIAL VELOCITIES	VAPOR	UGI= 0.0	LIQUID	ULI= 0.0
SOLID PARTICLE RADII	FUEL	RPSFI= 0.50000D-05	STEEL	RPSSI= 0.50000D-04

INPUT FOR MESH POINT SET 4

MESH POINT SET DESCRIPTION ****** MESH CELL SET 4 : SLIDING DOORS ******

MESH POINT SET BOUNDARIES BOTTOM (NB)= 6 TOP (NT)= 6 LEFT (NL)= 1 RIGHT (NR)= 5
IINP= 1 VAPOR DENSITIES AND TEMPERATURE INPUT--VAPOR PRESSURE DETERMINED
ISAT= 0 LIQUID TEMPERATURE DETERMINED BY INPUT DATA
IPAREG= 5 PARAMETER REGION NUMBER
ICELWS= 0 NUMBER OF COMPOSITION PARAMETERS TO HAVE THEIR VALUES INPUT MESH CELLWISE

MESH POINT SET DENSITIES AND TEMPERATURES

COMPONENT NUMBER N	STRUCTURE MACROSCOPIC DENSITY RSBRI(N)	STRUCTURE TEMPERATURE TSI(N)	LIQUID MACROSCOPIC DENSITY RLBRI(N)	LIQUID TEMPERATURE TLI(N)	VAPOR MICROSCOPIC DENSITY ROGI(N)
1	0.0	0.29300D+03	0.0	0.29300D+03	0.0
2	0.0	0.29300D+03	0.0	0.29300D+03	0.0
3	0.0	0.29300D+03	0.0	0.29300D+03	0.0
4	0.0	0.29300D+03	0.99300D-01	0.29300D+03	0.78676D-03
5	0.0	0.29300D+03	0.0	0.29300D+03	0.0
6	0.0		0.0	0.29300D+03	0.11620D+01
7	0.0		0.0		
8	0.0		0.0		
9	0.0				

VAPOR STATE	TEMPERATURE	TGI= 0.29300D+03	PRESSURE	PNI= 0.0
AXIAL VELOCITIES	VAPOR	VGI= 0.0	LIQUID	VLI= 0.0
RADIAL VELOCITIES	VAPOR	UGI= 0.0	LIQUID	ULI= 0.0
SOLID PARTICLE RADII	FUEL	RPSFI= 0.50000D-05	STEEL	RPSSI= 0.50000D-04

INPUT FOR MESH POINT SET 5

MESH POINT SET DESCRIPTION ****** MESH CELL SET 5: REFLECTOR REGION **********

MESH POINT SET BOUNDARIES BOTTOM (NB)= 9 TOP (NT)= 10 LEFT (NL)= 6 RIGHT (NR)= 8
IINP= 1 VAPOR DENSITIES AND TEMPERATURE INPUT--VAPOR PRESSURE DETERMINED
ISAT= 0 LIQUID TEMPERATURE DETERMINED BY INPUT DATA
IPAREG= 2 PARAMETER REGION NUMBER
ICELWS= 0 NUMBER OF COMPOSITION PARAMETERS TO HAVE THEIR VALUES INPUT MESH CELLWISE

MESH POINT SET DENSITIES AND TEMPERATURES

COMPONENT NUMBER N	STRUCTURE MACROSCOPIC DENSITY RSBRI(N)	STRUCTURE TEMPERATURE TSI(N)	LIQUID MACROSCOPIC DENSITY RLBRI(N)	LIQUID TEMPERATURE TLI(N)	VAPOR MICROSCOPIC DENSITY ROGI(N)
1	0.0	0.29300D+03	0.0	0.29300D+03	0.0
2	0.0	0.29300D+03	0.0	0.29300D+03	0.0
3	0.0	0.29300D+03	0.0	0.29300D+03	0.0
4	0.0	0.29300D+03	0.10000D+02	0.29300D+03	0.73993D+00
5	0.64075D+04	0.29300D+03	0.0	0.29300D+03	0.0
6	0.81015D+03		0.0	0.29300D+03	0.0
7	0.0		0.0		
8	0.0		0.0		
9	0.0				

VAPOR STATE	TEMPERATURE	TGI= 0.29300D+03	PRESSURE	PNI= 0.0
AXIAL VELOCITIES	VAPOR	VGI= 0.0	LIQUID	VLI= 0.0
RADIAL VELOCITIES	VAPOR	UGI= 0.0	LIQUID	ULI= 0.0
SOLID PARTICLE RADII	FUEL	RPSFI= 0.50000D-05	STEEL	RPSSI= 0.50000D-04

INPUT FOR MESH POINT SET 6

MESH POINT SET DESCRIPTION ****** MESH CELL SET 6 : SHIELDING TANK **********

MESH POINT SET BOUNDARIES BOTTOM (NB)= 9 TOP (NT)= 22 LEFT (NL)= 14 RIGHT (NR)= 16
IINP= 1 VAPOR DENSITIES AND TEMPERATURE INPUT--VAPOR PRESSURE DETERMINED
ISAT= 0 LIQUID TEMPERATURE DETERMINED BY INPUT DATA
IPAREG= 2 PARAMETER REGION NUMBER
ICELWS= 0 NUMBER OF COMPOSITION PARAMETERS TO HAVE THEIR VALUES INPUT MESH CELLWISE

MESH POINT SET DENSITIES AND TEMPERATURES

COMPONENT NUMBER N	STRUCTURE MACROSCOPIC DENSITY RSBRI(N)	STRUCTURE TEMPERATURE TSI(N)	LIQUID MACROSCOPIC DENSITY RLBRI(N)	LIQUID TEMPERATURE TLI(N)	VAPOR MICROSCOPIC DENSITY ROGI(N)
1	0.0	0.29300D+03	0.0	0.29300D+03	0.0
2	0.0	0.29300D+03	0.0	0.29300D+03	0.0
3	0.0	0.29300D+03	0.0	0.29300D+03	0.0
4	0.0	0.29300D+03	0.10000D+02	0.29300D+03	0.73993D+00
5	0.64075D+04	0.29300D+03	0.0	0.29300D+03	0.0
6	0.81015D+03		0.0	0.29300D+03	0.0
7	0.0		0.0		
8	0.0		0.0		
9	0.0				

VAPOR STATE	TEMPERATURE	TGI= 0.29300D+03	PRESSURE	PNI= 0.0
AXIAL VELOCITIES	VAPOR	VGI= 0.0	LIQUID	VLI= 0.0
RADIAL VELOCITIES	VAPOR	UGI= 0.0	LIQUID	ULI= 0.0
SOLID PARTICLE RADII	FUEL	RPSFI= 0.50000D-05	STEEL	RPSSI= 0.50000D-04

INPUT FOR MESH POINT SET 7

MESH POINT SET DESCRIPTION ****** MESH CELL SET 7 : COVER GAS VOLUME ******

MESH POINT SET BOUNDARIES BOTTOM (NB)= 29 TOP (NT)= 41 LEFT (NL)= 1 RIGHT (NR)= 19
IINP= 1 VAPOR DENSITIES AND TEMPERATURE INPUT--VAPOR PRESSURE DETERMINED
ISAT= 0 LIQUID TEMPERATURE DETERMINED BY INPUT DATA
IPAREG= 3 PARAMETER REGION NUMBER
ICELWS= 0 NUMBER OF COMPOSITION PARAMETERS TO HAVE THEIR VALUES INPUT MESH CELLWISE

MESH POINT SET DENSITIES AND TEMPERATURES

COMPONENT NUMBER N	STRUCTURE MACROSCOPIC DENSITY RSBRI(N)	STRUCTURE TEMPERATURE TSI(N)	LIQUID MACROSCOPIC DENSITY RLBRI(N)	LIQUID TEMPERATURE TLI(N)	VAPOR MICROSCOPIC DENSITY ROGI(N)
1	0.0	0.29300D+03	0.0	0.29300D+03	0.0
2	0.0	0.29300D+03	0.0	0.29300D+03	0.0
3	0.0	0.29300D+03	0.0	0.29300D+03	0.0
4	0.0	0.29300D+03	0.99300D-01	0.29300D+03	0.78676D-03
5	0.0	0.29300D+03	0.0	0.29300D+03	0.0
6	0.0		0.0	0.29300D+03	0.11620D+01
7	0.0		0.0		
8	0.0		0.0		
9	0.0				

VAPOR STATE	TEMPERATURE	TGI= 0.29300D+03	PRESSURE	PNI= 0.0
AXIAL VELOCITIES	VAPOR	VGI= 0.0	LIQUID	VLI= 0.0
RADIAL VELOCITIES	VAPOR	UGI= 0.0	LIQUID	ULI= 0.0
SOLID PARTICLE RADII	FUEL	RPSFI= 0.50000D-05	STEEL	RPSSI= 0.50000D-04

INPUT FOR MESH POINT SET 8

MESH POINT SET DESCRIPTION ****** MESH CELL SET 8 : DIPPLATE SUPPORT **********

MESH POINT SET BOUNDARIES BOTTOM (NB)= 25 TOP (NT)= 38 LEFT (NL)= 12 RIGHT (NR)= 14

IINP= 1 VAPOR DENSITIES AND TEMPERATURE INPUT--VAPOR PRESSURE DETERMINED

ISAT= 0 LIQUID TEMPERATURE DETERMINED BY INPUT DATA

IPAREG= 2 PARAMETER REGION NUMBER

ICELWS= 0 NUMBER OF COMPOSITION PARAMETERS TO HAVE THEIR VALUES INPUT MESH CELLWISE

MESH POINT SET DENSITIES AND TEMPERATURES

COMPONENT NUMBER N	STRUCTURE MACROSCOPIC DENSITY RSBRI(N)	STRUCTURE TEMPERATURE TSI(N)	LIQUID MACROSCOPIC DENSITY RLBRI(N)	LIQUID TEMPERATURE TLI(N)	VAPOR MICROSCOPIC DENSITY ROGI(N)
1	0.0	0.29300D+03	0.0	0.29300D+03	0.0
2	0.0	0.29300D+03	0.0	0.29300D+03	0.0
3	0.0	0.29300D+03	0.0	0.29300D+03	0.0
4	0.0	0.29300D+03	0.10000D+02	0.29300D+03	0.73993D+00
5	0.64075D+04	0.29300D+03	0.0	0.29300D+03	0.0
6	0.81015D+03		0.0	0.29300D+03	0.0
7	0.0		0.0		
8	0.0		0.0		
9	0.0				

VAPOR STATE	TEMPERATURE	TGI= 0.29300D+03	PRESSURE	PNI= 0.0
AXIAL VELOCITIES	VAPOR	VGI= 0.0	LIQUID	VLI= 0.0
RADIAL VELOCITIES	VAPOR	UGI= 0.0	LIQUID	ULI= 0.0
SOLID PARTICLE RADII	FUEL	RPSFI= 0.50000D-05	STEEL	RPSSI= 0.50000D-04

INPUT FOR MESH POINT SET 9

MESH POINT SET DESCRIPTION ****** MESH CELL SET 9 : GAP ABOVE SUPPORT ******

MESH POINT SET BOUNDARIES BOTTOM (NB)= 39 TOP (NT)= 41 LEFT (NL)= 12 RIGHT (NR)= 14
IINP= 1 VAPOR DENSITIES AND TEMPERATURE INPUT--VAPOR PRESSURE DETERMINED
ISAT= 0 LIQUID TEMPERATURE DETERMINED BY INPUT DATA
IPAREG= 2 PARAMETER REGION NUMBER
ICELWS= 0 NUMBER OF COMPOSITION PARAMETERS TO HAVE THEIR VALUES INPUT MESH CELLWISE

MESH POINT SET DENSITIES AND TEMPERATURES

COMPONENT NUMBER N	STRUCTURE MACROSCOPIC DENSITY RSBRI(N)	STRUCTURE TEMPERATURE TSI(N)	LIQUID MACROSCOPIC DENSITY RLBRI(N)	LIQUID TEMPERATURE TLI(N)	VAPOR MICROSCOPIC DENSITY ROGI(N)
1	0.0	0.29300D+03	0.0	0.29300D+03	0.0
2	0.0	0.29300D+03	0.0	0.29300D+03	0.0
3	0.0	0.29300D+03	0.0	0.29300D+03	0.0
4	0.0	0.29300D+03	0.99300D-01	0.29300D+03	0.78676D-03
5	0.18378D+04	0.29300D+03	0.0	0.29300D+03	0.0
6	0.23262D+03		0.0	0.29300D+03	0.11620D+01
7	0.0		0.0		
8	0.0		0.0		
9	0.0				

VAPOR STATE	TEMPERATURE	TGI= 0.29300D+03	PRESSURE	PNI= 0.0	
AXIAL VELOCITIES	VAPOR	VGI= 0.0	LIQUID	VLI= 0.0	
RADIAL VELOCITIES	VAPOR	UGI= 0.0	LIQUID	ULI= 0.0	
SOLID PARTICLE RADII	FUEL	RPSFI= 0.50000D-05	STEEL	RPSSI= 0.50000D-04	

INPUT FOR MESH POINT SET 10

MESH POINT SET DESCRIPTION **** MESH CELL SET 10 - DIP PLATE

MESH POINT SET BOUNDARIES BOTTOM (NB)= 25 TOP (NT)= 26 LEFT (NL)= 1 RIGHT (NR)= 14
IINP= 1 VAPOR DENSITIES AND TEMPERATURE INPUT--VAPOR PRESSURE DETERMINED
ISAT= 1 LIQUID TEMPERATURE NOT ALLOWED GREATER THAN THE SATURATION TEMPERATURE
IPAREG= 6 PARAMETER REGION NUMBER
ICELWS= 0 NUMBER OF COMPOSITION PARAMETERS TO HAVE THEIR VALUES INPUT MESH CELLWISE

MESH POINT SET DENSITIES AND TEMPERATURES

COMPONENT NUMBER N	STRUCTURE MACROSCOPIC DENSITY RSBRI(N)	STRUCTURE TEMPERATURE TSI(N)	LIQUID MACROSCOPIC DENSITY RLBRI(N)	LIQUID TEMPERATURE TLI(N)	VAPOR MICROSCOPIC DENSITY ROGI(N)
1	0.0	0.0	0.0	0.0	0.0
2	0.0	0.0	0.0	0.0	0.0
3	0.0	0.29300D+03	0.0	0.29300D+03	0.0
4	0.0	0.29300D+03	0.40000D+03	0.0	0.40000D-02
5	0.73650D+01	0.0	0.0	0.0	0.0
6	0.73650D+01		0.0	0.0	0.93000D+00
7	0.0		0.0		
8	0.0		0.0		
9	0.0				

VAPOR STATE	TEMPERATURE	TGI= 0.29300D+03	PRESSURE	PNI= 0.0
AXIAL VELOCITIES	VAPOR	VGI= 0.0	LIQUID	VLI= 0.0
RADIAL VELOCITIES	VAPOR	UGI= 0.0	LIQUID	ULI= 0.0
SOLID PARTICLE RADII	FUEL	RPSFI= 0.10000D-03	STEEL	RPSSI= 0.10000D-02

APPENDIX B: SUMMARY OF THE EVALUATION PROCEDURE

(1) Run SIMMER-II calculation (possibly with some restarts); store hydrodynamic postprocessor file and summation print out on two tapes.

(2) Interpolate postprocessor file to uniform time step of dt=2.0E-2ms; select the variables of interest; this is done using program POSTPROC[1].

(3) Restructure the summation print file using program SUMRED[1] to the format suitable for subsequent evaluations by program SUMPROC[1].

(4) Interpolate spatially the file created in (2) to the positions where transducers are located in the experiment (using PROSID code [2]).

(5) Using POSTPROC[1] again, create a primary file containing the local variables (pressure, volume fractions, velocities etc.) at the measurement positions as functions of time.

(6) Using SUMPROC[1], add to primary file the integral variables of interest (peak pressure, impulse to the head, etc.).

(7) Using program PROSID[2], add to primary file bubble volume, displaced volume and cover gas volume as function of time.

(8) Use program MODEASY[3] to calculate from primary file secondary quantities (such as impulse traces, energy conversion, etc.).

(9) Perform time synchronisation between experiment and calculation (again using MODEASY[3]).

(10) Plot calculational results against experimental curves using

the plotting package PLOTEASY[4].

(11) Plot calculational results as multidimensional plots using program HYDPLOT[5].

(12) At various stages of the evaluation it may be helpful to print out variables as function of space and/or time (using programs POSTPROC and SUMPROC[1]).

References to Programs Used for the Evaluation

[1] K.Küfner, POSTPROC, SUMRED, SUMPROC, unpublished internal program description (1982)

[2] R.Heger, K.Küfner, W.Maschek, PROSID, unpublished internal program description (1983)

[3] R.Heger, K.Küfner, MODEASY code documentation, unpublished internal program description (1982), publication as KFK report in preparation.

[4] C.Broeders, PLOTEASY, unpublished internal program description (1977)

[5] S.Kleinheins, HYDPLOT, unpublished internal program description (1980)